OPTICAL QUANTIFICATION OF HEMOLYSIS, ICTERUS, AND LIPEMIA IN HUMAN SERUM

by

Vimal Kumar Kasagani

A thesis submitted to the faculty of
The University of Utah
in partial fulfillment of the requirements for the degree of

Master of Science

Department of Mechanical Engineering

The University of Utah

December 2013

The University of Utah Graduate School

STATEMENT OF THESIS APPROVAL

The thesis of **Vimal Kumar Kasagani**

has been approved by the following supervisory committee members:

Eberhard Bamberg	, Chair	**03/22/2012** Date Approved
Stacy Morris Bamberg	, Member	**03/22/2012** Date Approved
Mathieu Francoeur	, Member	**03/22/2012** Date Approved

and by **Timothy Ameel** , Chair/Dean of

the Department/College/School of **Mechanical Engineering**

and by David B. Kieda, Dean of The Graduate School.

ABSTRACT

In order to increase the automation and efficiency for a national reference laboratory, the ability to quantify interferences like Hemolysis, Icterus, and Lipemia in serum samples is investigated. The system is intended as a screening step prior to clinical analysis of medical samples to prevent false results caused by the interferences. The system is based on selective absorption of transmitted light by the interferences that cause loss of light at specific wavelengths. The absorption spectra of interferences are analyzed to identify the appropriate wavelengths, resulting in a mathematical formulation between the absorbance and concentrations. An absorption wavelength is selected so that the transmitted power of light through a tube with the sample significantly decreased due to the presence of condition of interest, while the reference wavelength is selected so that the transmitted light varies mostly due to the presence of tube material and labels and does not vary due to the presence of interference.

A computational model is formulated using a commercial software package, ANSYS FLUENT, in order to understand the absorption and scattering effects, the thermal effects of higher power irradiation on the biological samples, as well as to determine the radiant power of transmitted light through the sample for different power levels. The Discrete Ordinates Method is used to model the radiation through a participating medium. The temperature distribution and spectral power of transmitted radiation are determined for water in a tube for different wavelengths used in the current system.

TABLE OF CONTENTS

ACKNOWLEDGEMENTS

First, I would like to express my deepest appreciation to my advisor, Dr. Eberhard Bamberg, for giving me this platinum opportunity. His attitude, substance of genius, and persevering support as my advisor has boosted my confidence. I would like to thank Dr. Stacy Bamberg and Dr. Mathieu Francoeur for being a part of my supervisory committee and for their valuable suggestions. I would like to especially thank Dr. Mathieu Francoeur for his immense support and guidance throughout the second phase of the project. I would like to thank ARUP Laboratories for being the financial backbone for this research. I would like to thank Dr. Charles Hawker and Dr. William Roberts for their expertise in testing medical samples and particular thanks to William Owen for providing and characterizing the medical samples used in this research.

I would like to thank my colleague, Dr. Xin Liu, for his help in understanding the project. I would like to express my gratitude towards Shashank Pandey for his time in the research discussions. Also I would like to thank my close friends and roommates for their moral support.

The section would be incomplete without mentioning the most important persons in my life – my parents and my siblings who confided in me and brought me up to this stage; Thank you Mom and Dad. Thank you Veni and Rakhi. Above all of us, I would like to thank the God Almighty for giving me the strength and courage to face all the challenges.

CHAPTER 1

INTRODUCTION

1.1 Background

ARUP Laboratories is a national clinical and anatomic pathology reference laboratory located in Salt Lake City, Utah. It receives 40,000 – 45,000 medical samples on an average per day from different parts of the U.S and is one of the most automated laboratories in the country. It uses automated storage and retrieval system (AR/RS) to transport, store, and retrieve the large number of specimens. To centralize high volume testing, ARUP began the Automated Core Laboratory (ATL). With more than 130 different tests performed, it is the largest and busiest laboratory section, in which 95 percent of the tests performed are reported within 24 hours. Eighty percent of these tests are automated, while the remaining tests are performed manually by experienced technicians [1][2].

To improve the quality of testing and reduce labor cost and the turn-around time, ARUP is striving to develop cutting edge automation. One such system is the optical volume detection system [3], which was already developed and is currently being used at ARUP Labs. The current work addresses quantification of interferences in serum samples.

1.1.1 Sample Containers and Labels

The most commonly used sample containers in ARUP labs are the polypropylene false bottom tubes with polyethylene screw caps, as shown in Figure 1.1. These polypropylene tubes are also called reagent or centrifuge tubes. Each tube can hold a maximum volume of 5 mL and has a volume scale up to 4 mL printed on the tube. The tubes are covered with an unknown number of polyurethane labels. The labels have a barcode printed on them, which is specific for each sample and provide information such as the contents of sample, the patient details, and the testing facility. In the extreme case, there can be three labels stacked on one side of the tube and three more on the other side, completely covering the tube [1].

1.1.2 Volume Detection

One of the automation requirements at ARUP was to determine the minimum and maximum liquid levels of samples in the test tubes. A novel opto-mechanical system was developed for liquid level detection of medical samples in tubes that are covered by an unknown number of labels. The power ratio of transmitted light for two different wavelengths is computed and compared to a threshold value to detect the liquid level. Through a series of experiments, the system was developed to detect the liquid level with an uncertainty of 0.1 mL, with a confidence level of 99.73% and with a total test time of 0.5 seconds. These results were attained when the outside of test tubes were covered with up to six layers of labels [4]. With these characteristics, a laboratory proto-type was built for its use in ARUP labs.

Further, to determine the volume of liquid accurately, the shape and position of meniscus was considered. Experiments with the volume detection system found that it

could measure the volume of liquid in standard test tubes with an uncertainty of 0.06 mL and with a confidence level of 99.73% [5].

1.1.3 Interference Detection and Quantification

Interferences in serum and plasma samples affect the quality of analysis in immunologic tests and serum chemistry tests. Specimens may contain interferences such as Hemolysis, Icterus, and Lipemia. Serum samples in test tubes with the different interferences are shown in Figure 1.2.

- Hemolysis is the breakage of the red blood cells' membrane, causing the release of the hemoglobin and other internal components into the surrounding fluid. Hemolysis is visually detected by showing a pink to red tinge in serum or plasma [6].
- Icterus is a yellowish discoloration of the skin that is caused by increased levels of bilirubin (produced by liver) in the blood [7].
- Lipemia is one of the most commonly encountered components that cause interference in clinical laboratory testing. Excess introduction of lipids like fats, oils, sterols, and esters into the blood results in Lipemia [8].

The measurement requirements of these interferences depend on the tests that are ordered for the patient [1]. Some assays are interfered at very high concentrations while some assays are interfered at much lower concentrations. Based on the possible concentrations of these interferences, samples were prepared by ARUP Labs. The concentration range of interferences in serum samples that were provided by ARUP are as listed in Table 1.1.

1.2 Contributions

Through a series of experiments followed by data analysis, an optical system was developed to measure concentrations of Hemolysis up to 1250 mg/dL, Icterus up to 60 mg/dL, and Lipemia up to 707 mg/dL for human serum samples in test tubes without labels.

To understand the absorption and scattering effects and to model temperature distribution and transmitted power of radiation for a liquid sample irradiated by a laser beam, a radiative heat transfer model coupled with energy equation is formulated. The results of transmitted radiation through a water sample were experimentally validated for the current laser light sources in use.

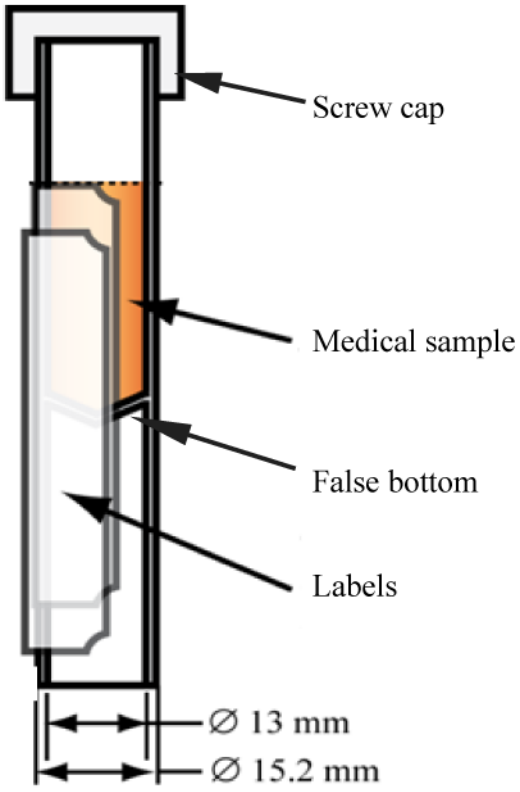

Figure 1.1 Polypropylene test tube used in ARUP Labs [3]

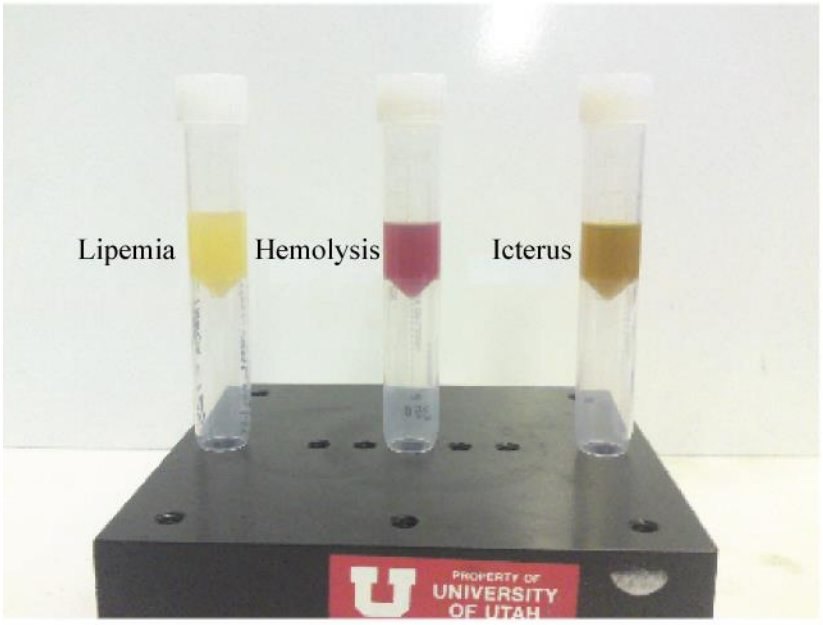

Figure 1.2 Test tubes with serum samples containing interferences

Table 1.1 Range of interference concentrations in serum samples provided by ARUP Labs

Interference	**Concentration range (mg/dL)**
Hemolysis	0 – 1250
Icterus	0 – 60
Lipemia	0 – 707

CHAPTER 2

LITERATURE SURVEY

2.1 Current State of Art

At present, medical samples are examined visually by skilled laboratory personnel based on the color of the sample. For example, a serum sample with an excess of hemoglobin is reddish in color, a serum sample with an excess of bilirubin has a yellow-green color, and a sample containing lipids is whitish in color [9]. Numerous labels that cover the tube block all the visible access into the tube. So to estimate the color of the specimen, the technician would have to unscrew the cap of the tube and look down into it. This is not an ideal solution because it exposes the technician to unknown contents of the tube and subjects the contents of the tube to possible contamination. Moreover, the visual inspection is labor-intensive and the results are highly subjective.

2.2 Existing Literature

Melvin et al. examined the frequency for Hemolysis, Icterus, and Lipemia in 2599 serum samples which were submitted for chemistry testing. To assess the accuracy of visual inspection, the concentrations of hemoglobin, bilirubin, and triglycerides in the specimens considered to be contaminated were determined and compared with the visual grading of experienced technical personnel. It was found that there was little agreement between the actual concentration and the assigned grade of interferences, confirming the human visual estimation of interferences as unreliable [10].

Rovati and Docchio developed a solid-state colorimeter to determine the concentrations of Hemolysis, Icterus, and Lipemia interferences. The method was based on measurement of extinction coefficients of serum with interference samples at special wavelengths. It used LEDs emitting to the glass tubes with interferences and collected the scattered light at an angle of 45 degrees. The system reported concentration measurements of up to 318 mg/dL for Hemolysis, 22 mg/dL for Icterus, and 450 A.U (arbitrary unit) for Lipemia for samples contained in glass tubes without labels attached on the outside [9].

Gunasekaran and Sankari used a spectroscopic absorption technique to study the spectral differences between a healthy serum and those affected by some diseases. The absorbance was directly proportional to the concentration. The different serum samples were analyzed quantitatively by calculating the intensity ratio among the absorption peaks. However, no paper labels were affixed to the test tubes [11].

Kanagathara et al. suggested the use of spectroscopic techniques like Fourier Transform Infrared (FTIR) and Ultraviolet (UV) in the analysis of blood serum for determination of diseases in human body. A linear relationship was found between the protein content and the maximum absorption spectrum in UV region. FTIR spectrum was used to determine the molecular finger print out which was compared to the clinical test for diagnostic purpose [12].

Ranganathan and Gunasekaran investigated a method that replaced the subjective human perception of color with a nonsubjective machine vision system based on artificial neural networks. The system revealed a strong relation between the color of the blood sample and the level of hemoglobin. The system was capable of estimating the

hemoglobin in human blood to 16.5 mg/dL. [13]. Luoma et al. described the Abbott HIL feature on the ARCHITECT Clinical Chemistry c8000 and c16000 systems that was developed to provide objective measurements of sample quality via qualitative and or unitless semiquantitative index measurements that correspond to the amount of Hemolysis, Icterus, and Lipemia in patient specimens. The results were determined by differential optical measurements [14]. However, the system required the removal of the test tube cap.

Neudel and Takatani used an integrated optical sensor working at three specific wavelengths to measure the reflected light. The increase of free hemoglobin in plasma led to a decrease of detected reflected light at all three wavelengths [15].

Sankai et al. developed a combination of laser diode and optical spectrum analyzer to obtain a greater accuracy compared to the colorimetric method to measure hemolysis in each sample. An adequate correlation between the continuous laser measurement data and the sample data was found [16].

Fine et al. were issued United States Patent 6,711,424 which uses at least two wavelengths of light to determine the interferences in blood. The light intensities measured are plotted and the slope is calculated and compared to predetermined curves of known conditions. This device would not work for ARUP labs as different label combinations require different curves for comparison [17].

Based on the current literature, a device capable of satisfying ARUP's needs has not been developed.

CHAPTER 3

OPTICAL QUANTIFICATION OF INTERFERENCES IN SERUM

3.1 Introduction

This chapter describes the principle of quantification of interferences in medical samples, different experiments conducted, and the analysis of results obtained from the experiments. The principle used in this system was developed from the Beer-Lambert law. First, the spectral absorption of the interferences was obtained by transmitting light from a white light source through the test tube containing serum with interferences like Hemolysis, Icterus, and Lipemia. The optical signatures were analyzed to identify the reference and absorption wavelengths to select the appropriate Laser Diodes (LDs) and LEDs that were used in the measurement system. Using these LDs and LEDs, meaningful measurement results of interferences were obtained.

3.2 Beer-Lambert Law

Absorption of a beam of light passing through a medium causes the radiant power of the light to become attenuated. According to the Beer–Lambert law illustrated in Figure 3.1, the transmission of a medium can be expressed as the ratio of the radiant power of light exiting the medium to the radiant power of light entering the medium. Furthermore, there exists a logarithmic dependence between the transmission and the product of the absorption coefficient of the substance and the distance the light travels through the material. The absorption coefficient can be written as the product of the molar

absorptivity of the absorber and the concentration of the absorbing species in the medium. The Beer–Lambert law is written as [18] [19],

$$T = \frac{P_1}{P_0} = 10^{-\alpha l} = 10^{-\varepsilon c l} \tag{3.1}$$

where T = Transmittance

P_0 = Radiant power of incident light [W]

P_1 = Radiant power of transmitted light [W]

α = Absorption coefficient of the medium [1/m]

l = Distance through which light travels in the absorbing medium [m]

ε = Molar absorptivity of absorber [m2/mol]

c = Concentration of absorbing species [mol/m3]

The molar absorptivity is an intrinsic property of a medium which is defined as the capacity of the medium to absorb light at a given wavelength. The absorbance A is expressed in terms of the transmission T, which for liquids is defined as [19]

$$A = -\log_{10}(T) = -\log_{10}\left(\frac{P_1}{P_0}\right) = \alpha l = \varepsilon c l \tag{3.2}$$

This means that absorbance depends linearly with the concentration of the medium.

3.3 Spectral Absorption of Interferences

The initial step in developing the system was to study the absorption spectra of the interferences. The main idea of the experiment is to irradiate or illuminate the specimen of interest using a white light source and capture the transmitted light at the other end using an optical spectrum analyzer (OSA) to obtain the optical signatures over a wavelength range.

3.3.1 Experimental Set-up

The light source used was a 150 Illuminator from Ram Optical Instrumentation Inc. (ratings: 120VAC, 60Hz, 2.5Amp Fuse) shown in Figure 3.2. A halogen bulb of the type EJV (ratings: 150 Watt, 21Volt, 40 hours rated life) was used in the illuminator which has a built-in lamp holder that holds the bulb. A VIS-NIR (Visible to Near Infrared) Optical Fiber Cable (1000µm Core, 1250µm Clad, 1m Length, SMA from Newport, model 78302) was connected to the light source and this cable terminates with a Newport collimating probe (model 78332) to obtain parallel rays. The collimated light from the optical fiber was passed through a bi-convex lens from a Newport model (KBX046) to focus on to the polypropylene test tube which was set at the focal point of the lens. The light coming out of the tube was passed through another bi-convex lens and focused onto another optical fiber that is connected to an ANDO AQ6315E Optical Spectrum Analyzer, shown in Figure 3.3. The OSA can measure the light intensity as a function of wavelength from 350 nm to 1750 nm with a desired resolution. A LabVIEW script was developed to communicate with the analyzer that is connected to the computer through a GPIB (General purpose Interface Bus) to USB (Universal Serial Bus) interface to record the intensities and save it as a text file in the computer

3.3.2 Alignment

The alignment of the optical fibers, the focusing optics (bi-convex lens), and the test tube in X, Y, Z, and θ directions is very important to retain maximum light coming from the light source. This was achieved by using the posts on manual linear translational stages that are mounted on the track, as shown in the Figure 3.4. The posts offer movement in the Z and θ directions, the translational stages offer movement in the Y

direction by means of a micrometer screw, and the movement in the X direction is achieved by moving the linear stages on the track. A special fixture designed for the false bottom of the polypropylene test tube holds it in position. The fixture was also mounted on other translation stages for its movements in the X, Y, and Z directions.

3.3.3 Experimental Procedure

Various samples of serum containing three different interferences of different concentration levels were collected from ARUP Laboratories. Prior to testing, the halogen white light source was allowed to warm up for 30 minutes. Using the experimental set-up described, each sample was scanned from 350 nm to 1150 nm with a resolution of 0.2 nm. The measured intensity of the transmitted light was averaged over 500 measurements per sample point using a LabVIEW code. Next, the test tube was replaced with a tube containing no-index serum, which is a sample that is absolutely free of any interference. To remove the effects of attenuation by the test tube, errors of the spectrum analyzer, and the nonuniform intensity of the white light source, the transmitted power is then normalized with the power transmitted through no-index serum. Under the same experimental conditions, samples of three interferences were scanned to study the optical response and the results were analyzed using a Matlab program.

3.3.4 Spectral Analysis for Hemolysis

Figure 3.5 shows the radiant power of transmitted light through serum samples with different concentration levels of Hemolysis. It shows that the decrease in transmitted radiant power with concentration is significant in the wavelength band of 400 nm to 600 nm compared to the wavelengths greater than 600 nm. For concentrations more than 313 mg/dL, the transmitted light was too low in the wavelength range 400 nm to 600 nm and

beyond the resolution of the spectrometer. To consider the absorption effects of the interference only, the transmitted power through various concentrations of Hemolysis is normalized with the transmitted power of light through a no-index serum or an interference free serum as per the equation,

$$P_N = \frac{P}{P_{no-index}} \tag{3.3}$$

where P_N is the power normalized

$P_{no-index}$ is the power transmitted through the interference free serum.

Figure 3.6 shows the normalized power against the wavelength for different concentrations of Hemolysis. The unreliable data below spectrometer limit were excluded while plotting the normalized powers.

From the equation (3.2), the absorption coefficient, α is calculated as

$$\alpha = -\frac{\log_{10}(P_N)}{L} \tag{3.4}$$

Here the path length, L, is the external diameter of the tube, which was measured using a vernier-calipers as 15.08 mm and P_N is the normalized power. From Figure 3.7, peaks near wavelengths 435, 540, and 575 nm indicate significant absorption when compared to the wavelengths longer than 600 nm, where the absorption does not vary significantly with the concentration.

3.3.5 Spectral Analysis for Icterus

Figure 3.8 shows the radiant power transmitted through the serum samples with different concentration levels of Icterus. For all the concentrations, the transmittance of white light is too low in the wavelength range of 400 nm to 500 nm compared to the wavelengths longer than 500 nm. Figure 3.9 shows the normalized power against the

wavelength for different concentrations of Icterus. There is a significant decrease in the normalized power with concentration in the wavelength range of 500 nm to 550 nm compared to the variation for remaining wavelengths. The absorption spectrum of Icterus at various concentrations is shown in Figure 3.10. Between wavelengths from 510 nm and 540 nm, the absorption coefficients increase with an increase in concentration. A drastic drop of the absorption coefficients is observed starting at a wavelength of about 600 nm.

3.3.6 Spectral Analysis of Lipemia

Figure 3.11 shows the radiant power of light transmitted through serum samples with different concentration levels of Lipemia. For concentrations starting from 238 mg/dL, in the wavelength range of 350 – 600 nm, the transmitted power is lower than the spectrometer measurement level so the data are considered unreliable for analysis. Figure 3.12 shows the normalized power against the wavelength for different concentrations of Lipemia. The power transmitted is normalized with the power through an interference free serum sample. Unlike Hemolysis and Icterus, the Lipemic samples do not exhibit distinct peaks in the absorption spectra. Instead the power is attenuated greatly by the presence of lipid particles between wavelengths 600 nm and 700 nm. Figure 3.13 shows that the absorption coefficients in the wavelength range 600 - 700 nm are greater than at 1000 nm.

3.3.7 Combined Spectral Analysis of Interferences

When a combined spectral absorption is analyzed, as shown in Figure 3.14, it is observed that Hemolysis, Icterus, and Lipemia have distinct absorption bands. This can

be used to detect and differentiate interferences apart from quantifying a specific interference.

3.4 Principle of Quantification

To understand the effect of absorption of interference, consider the interference itself as the only medium present and a beam of incident light passes through the medium, as shown in Figure 3.15. As seen from the plots of absorption coefficients, for each curve corresponding to a given concentration, the absorption is high at certain wavelengths and very low at some other wavelengths. This is due to the molar absorptivity, ε or molar absorption coefficient. Consider two wavelengths of light λ_a- absorption wavelength and λ_r- reference wavelength, such that the absorption of medium for λ_a is a constant value, absorption coefficient. Consider two wavelengths of light λ_a- absorption wavelength and λ_r- reference wavelength, such that the absorption of medium for λ_a is a constant value, and absorption for λ_r is negligible or zero. So from the equation (3.2), the absorbance of incident light at these wavelengths is given by

$$A_{\lambda_a} = -\log_{10}\left(\frac{P_{1,\lambda_a}}{P_{0,\lambda_a}}\right) = \alpha_{\lambda_a} L = \varepsilon_{\lambda_a} cL \tag{3.5}$$

$$A_{\lambda_r} = -\log_{10}\left(\frac{P_{1,\lambda_r}}{P_{0,\lambda_r}}\right) = \alpha_{\lambda_r} L = \varepsilon_{\lambda_r} cL \tag{3.6}$$

Since the incident power is the same in both the cases,

$$P_{0,\lambda_a} = P_{0,\lambda_r}$$

Since the absorption is negligible in case of λ_r,

$$P_{0,\lambda_r} \approx P_{1,\lambda_r}$$

So, $$P_{0,\lambda_a} \approx P_{1,\lambda_r}$$

Substituting this in equation (3.5),

$$A_{\lambda_a} \approx -\log_{10}\left(\frac{P_{1,\lambda_a}}{P_{1,\lambda_r}}\right) = \alpha_{\lambda_a} L = \varepsilon_{\lambda_a} c \tag{3.7}$$

where ε_{λ_a}, the molar absorption coefficient, is constant for a medium for a given wavelength and L, the path length, is also a constant. So a linear relation is observed between the concentration and absorbance or negative logarithm of transmitted power ratio for absorption and reference wavelengths ($-\log_{10}\left(\frac{P_{1,\lambda_a}}{P_{1,\lambda_r}}\right)$).

In reality, the medium consists of serum samples of interferences in a test tube covered with a number a labels (0 - 3) on the outside of the tube. To compensate the effect of tube material and geometry, labels etc., the absorption wavelength is selected such that the absorption coefficient significantly changes with the concentration while the reference wavelength is selected such that the change in absorption coefficient is negligible with concentration change. In other words, the absorption wavelength is selected at a wavelength where the transmitted power of light through the tube with the sample significantly decreased due to the presence of the condition of interest, while the reference wavelength is selected such that transmitted power of light varies mostly due to the tube material and labels but not the interference. Then, a standard linear fit relation is obtained from the known concentrations of the interferences that can be used to quantify any unknown concentration level of that interference.

3.5 Selection of Light Sources

From the plots of absorption coefficients of various interferences, combinations of absorption (λ_a) and reference (λ_r) wavelengths were selected according to the principle of detection and so that the absorption wavelengths are different for each interference. For these combinations, the power ratios of transmitted light through test tubes with the

samples are plotted against the concentrations of the corresponding interference. The equation for the best fit is provided, the norm of residuals, standard error, and the correlation coefficient were calculated to determine the goodness of the linear fit.

3.5.1 Power Ratios for Hemolysis

Figure 3.16 shows the linear fit relation between power ratios of Hemolysis for selected combinations of absorption and reference wavelengths λ_a and λ_r, respectively. The plot shows only up to 313 mg/dL as the transmitted light data for higher concentrations was unreliable. The linear fits for various combinations are compared using the slope obtained from the equation of the curve and the values of norm and correlation coefficient. Power ratios are calculated using the equation (3.7),

$$P_r = -\log_{10}\left(\frac{P_{1,\lambda_a}}{P_{1,\lambda_r}}\right)$$

3.5.2 Power Ratios for Icterus

Figure 3.17 shows the power ratios of Icterus for selected combinations of absorption and reference wavelengths plotted against concentrations.

3.5.3 Power Ratios for Lipemia

For various concentrations of Lipemia, good linear relation is observed between concentrations and power ratios for the selected combinations of absorption and reference wavelengths, as shown in Figure 3.18.

Considering the rules that the slope must be large and the correlation coefficient (r) should be close to 1, typical wavelengths for testing of Hemolysis, Icterus, and Lipemia were selected and laser light sources were searched for specific absorption and reference wavelengths in the market. Based on the availability, cost, and stability, LDs and LEDs

were selected for the application. LDs with wavelength 532 nm and 690 nm were selected to test Hemolysis with different concentrations. LEDs with peak wavelength 520 nm and 575 nm were used to test Icterus with different concentrations. Icterus has its special absorption spectrum in a domain, from 510 nm to 540 nm, but not in a single wavelength, as seen in Figure 3.10. LED has spectral bandwidth, which is larger than LD's, and so LED can be intelligently used in the testing of Icterus. LDs with wavelength 690 nm and 980 nm were selected to test Lipemia with different concentrations.

3.6 Quantification of Interferences Using LDs/LEDs and Detector

3.6.1 Experimental Set-up and Procedure

In these experiments, the light source used was the LD or LED selected. These LDs and LEDs come with a separate DC power source and a driver circuit board to control the operating mode and power output. The LDs and LEDs were used in collimated tubes with focusing lenses. The light from the LD or LED is focused onto the tube with serum sample that is placed in the path of the light beam using the same fixture as the one used in the spectral absorption experiment. The light passed through the tube was detected by a silicon detector PDA36A from Thorlabs. The detector is sensitive to light from 350 nm – 1100 nm with an active photodiode area of 3.6 x 3.6 mm (13 mm^2). The detector was connected to a data acquisition (DAQ) device NI USB 6211(16-Bit, 250 kS/s) using a coax cable. NI DAQ was connected to the computer using the USB interface and controlled using a LabVIEW script to obtain the intensities in terms of voltage signals. Figure 3.19 shows a schematic of the experimental set-up. The PDA36A photo detector has a built-in amplifier that is controlled by an eight-position rotary switch to vary the gain. The maximum output of the PDA36A is 10 volts, so the gain was adjusted so that

the measured signal is below 10 volts to avoid saturation. The serum samples with various levels of concentration of interferences were tested with their respective absorption and reference wavelength light sources. To compare the intensities of transmitted light for absorption and reference wavelengths, the voltages obtained at different gain levels are adjusted to the same gain using the trans-impedance gain values of the detector. Also, the optical output power of light sources for absorption and reference wavelengths are not the same, so the gain adjusted voltage signal for each measurement was normalized with direct light (without any tube in the light path) output through the corresponding light source. Using these measurements the power ratios were calculated to verify their linearity with concentrations.

From repeated experiments and analysis, it was observed that the following conditions were to be maintained in order to obtain reasonable results.

1. The light source LD or LED must be allowed to warm up for 10 to 15 minutes until there is a steady output.
2. To minimize the loss of intensity, the light source, test tube, and amplified detector were placed very close (less than 1 mm spacing) to each other and a focusing lens was used wherever necessary.
3. To minimize the effects of reflection, refraction, and scattering at the air-tube interface and tube-water interface, a circular laser beam of diameter 2 mm (approximately) was maintained in the measurements. The beam was focused normal to the tube wall and passing through its center. Scattering by the medium is one important factor that greatly affects the system and difficult to eliminate; it is evident from the fact that one can see the illumination of the sample from any

angle during the irradiation. The experimental set-up was covered with a shielded box in order to avoid any external noise and to maintain uniform ambience.

4. The white engravings (volume level indications) that are not uniformly distributed on the tube cause significant reflection of the light, so the tube was rotated such that no markings were in the path.

3.6.2 Measurement of Hemolysis

Figure 3.20 shows the voltage values for transmitted light obtained for different concentrations of Hemolysis for absorption and reference wavelengths λ_a=532 nm and λ_r=690 nm, respectively. The gain level at which the voltage is measured is indicated above the data points.

Using the gain factors of the detector, voltages at different gain levels are converted to voltage at 0 dB, $V_{0\ dB}$ as

$$V_{0\ dB} = TG_0/TG_n \tag{3.8}$$

where TG_0 and TG_n are the trans-impedance gain values at 0 dB and the gain at which that voltage is measured. Figure 3.21 shows the gain adjusted voltage values for Hemolysis.

The optical output powers of these light sources are unequal. So to compare the light intensities for absorption and reference wavelengths, the gain adjusted voltage values at 0 dB were normalized with voltage measured for direct light (without any tube in the light path) at 0 dB from the corresponding light source.

$$V_N = V_{0\ dB}/V_{direct\ light\ 0\ dB} \tag{3.9}$$

where V_N is the normalized voltage at 0 dB

$V_{0\ dB}$ is the voltage value measured at 0 dB

$V_{direct\ light\ 0\ dB}$ is the voltage value measured for direct light at 0 dB

Figure 3.22 shows the normalized voltage values for Hemolysis measurements. It is seen that the drop in transmitted light for 690 nm (reference) is comparatively less than that for 532 nm (absorption) as expected. For 532 nm, the decrease in transmitted light at higher concentrations is much less compared to that at lower concentrations.

According to the principle of detection, the power ratios are calculated as

$$P_r = -\log_{10}(V_{N\ 532}/V_{N\ 690}) \tag{3.10}$$

where P_r is the power ratio for Hemolysis

$V_{N\ 532}$ is the normalized voltage for absorption wavelength (532 nm)

$V_{N\ 690}$ is the normalized voltage for reference wavelength (690 nm)

Figure 3.23 shows the linearity between the concentrations and power ratios of Hemolysis. To show a good linear relation, the graph is plotted only up to 313 mg/dL. The expected linear relation deviates at higher concentrations. To show the relationship between concentrations and power ratios for higher concentrations of Hemolysis, a quadratic fit is described in Figure 3.24. So the polynomial fit is a better approximation to measure the concentrations over the complete range.

3.6.3 Measurement of Icterus

Figure 3.25 shows the voltage values for transmitted light obtained for different concentrations of Icterus for absorption and reference wavelengths λ_a=525 nm and λ_r=570 nm, respectively.

Figure 3.26 shows the gain adjusted voltage values for Icterus. Figure 3.27 shows the normalized voltage values for Icterus measurements. It is seen that for the complete range of concentrations, the drop in transmitted light for 570 nm (reference) is comparatively

less than that for 525 nm (absorption) as expected. Figure 3.28 shows the linearity between the concentrations and power ratios for Icterus. The expected linear relation holds good for the complete range of possible concentrations.

3.6.4 Measurement of Lipemia

Figure 3.29 shows the voltage values for transmitted light obtained for different concentrations of Lipemia for absorption and reference wavelengths λ_a=690 nm and λ_r=980 nm, respectively. Figure 3.30 shows the gain adjusted voltage values for Lipemia.

Figure 3.31 shows the normalized voltage values for Lipemia measurements. It is seen that for the complete range of concentrations, the drop in transmitted light for 570 nm (reference) is comparatively less than that for 525 nm (absorption) as expected.

Figure 3.32 shows the linearity between the concentrations and power ratios for Lipemia. To show a good linear relation, the graph is plotted only up to 559 mg/dL. The expected linear relationship deviates when extended up to 707 mg/dL.

To show the relationship between concentrations and power ratios for higher concentrations of Lipemia, a quadratic fit is described in Figure 3.33. So the polynomial fit is a better approximation to measure the concentrations over the complete range.

3.7 Discussion

From these experimental results, it is observed that the measurement system based on the Beer-Lambert law of linear dependence between absorbance and concentration works for low concentrations but deviates at higher concentrations. The possible errors from alignment, external noises, etc. have been minimized in the experimental set-up. During the experiments, it was observed that for high concentrations, illumination of the tube with samples was spread all around the tube unlike at low concentrations where most of

the light was concentrated in the direction where the detector was placed. This is due to the high scattering caused by suspended particles at high concentrations of interferences. The attenuation of light for highly scattering media cannot be described using the Beer-Lambert law [20]. Scattering effects are likely to play a dominant role in addition to absorption at higher concentrations so they must be accounted for to have accurate results. The absorption coefficient, α in equation (3.1) changes to the extinction coefficient, $\beta = (\alpha + \sigma_s)$ where σ_s is the scattering coefficient. The scattering can be isotropic or anisotropic, single scattering or multiscattering [21]. The scattering depends on a number of factors such as the size of particles suspended in solution, number of particles, and wavelength of light.

Another way to look at these deviations is that the Beer-Lambert law assumes that absorbing particles in medium behave independently with respect to light. In highly concentrated solutions when particles are lying in the same optical path such that some particles are in the shadow of others, error is introduced. For P_1/P_0 = 0.1 to 1, the measurements of absorption are less affected by shadowing than other sources of error so for high absorption coefficients, the concentrations are underestimated due to the shadow affect [19]. The exact explanation for interaction of cell particles in biological samples with the incident light is beyond the scope of the current research.

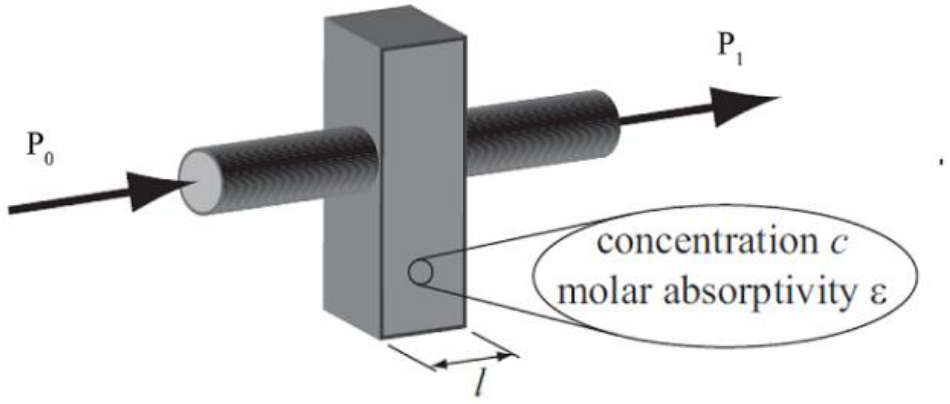

Figure 3.1 Beer–Lambert absorption of a beam of light as it travels through a medium [19].

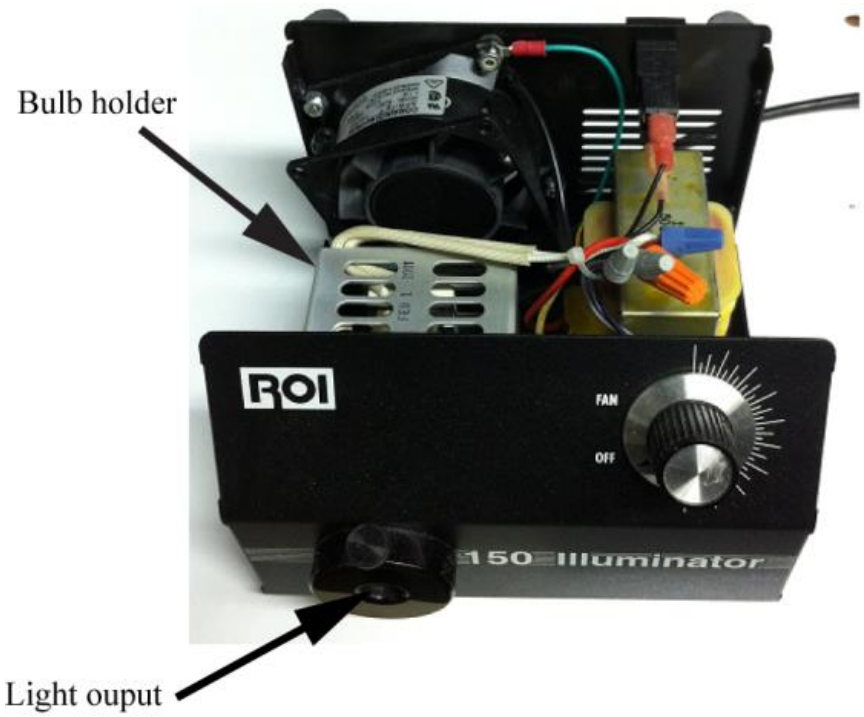

Figure 3.2 Open view of white light source.

Figure 3.3 Optical Spectrum Analyzer ANDO AQ6315E.

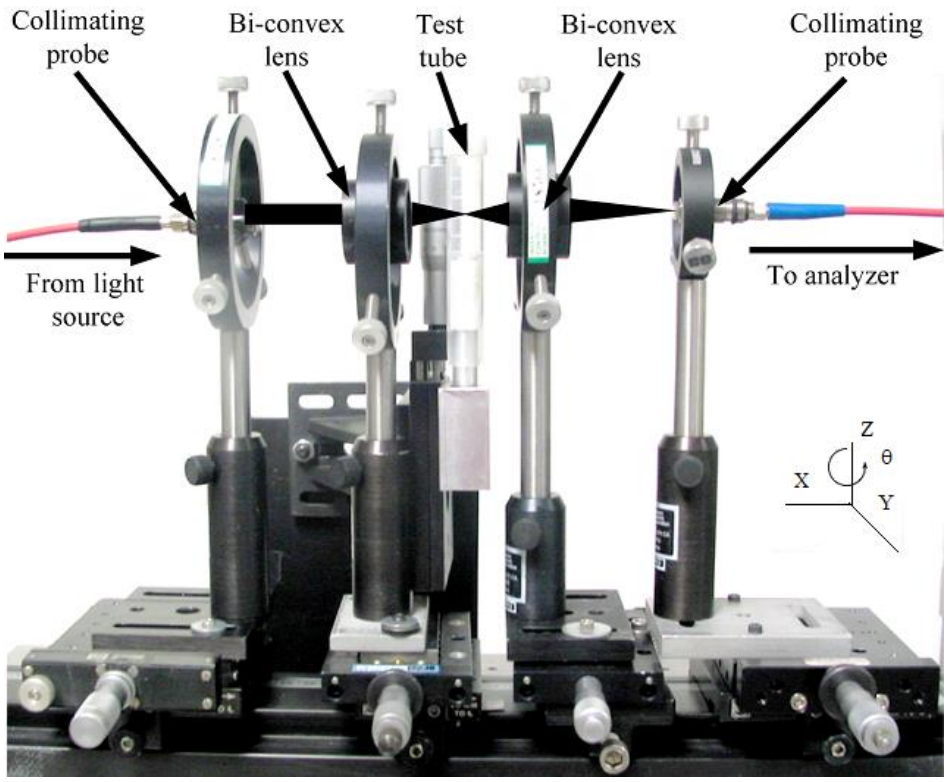

Figure 3.4 Experimental set-up to obtain absorption spectra of serum containing interferences.

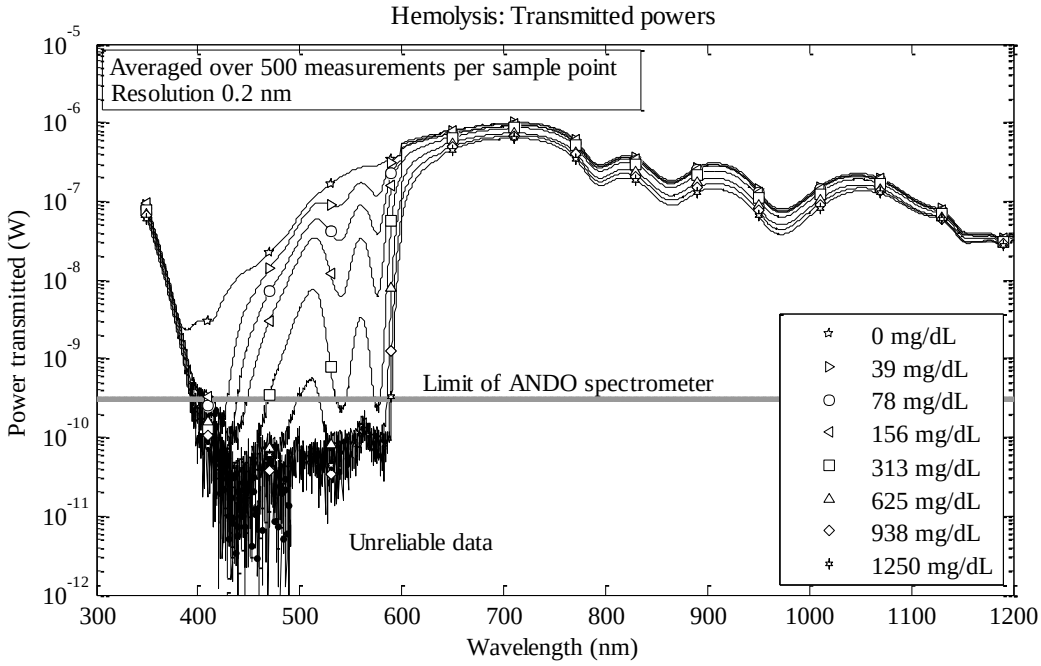

Figure 3.5 Power transmitted through serum samples with Hemolysis

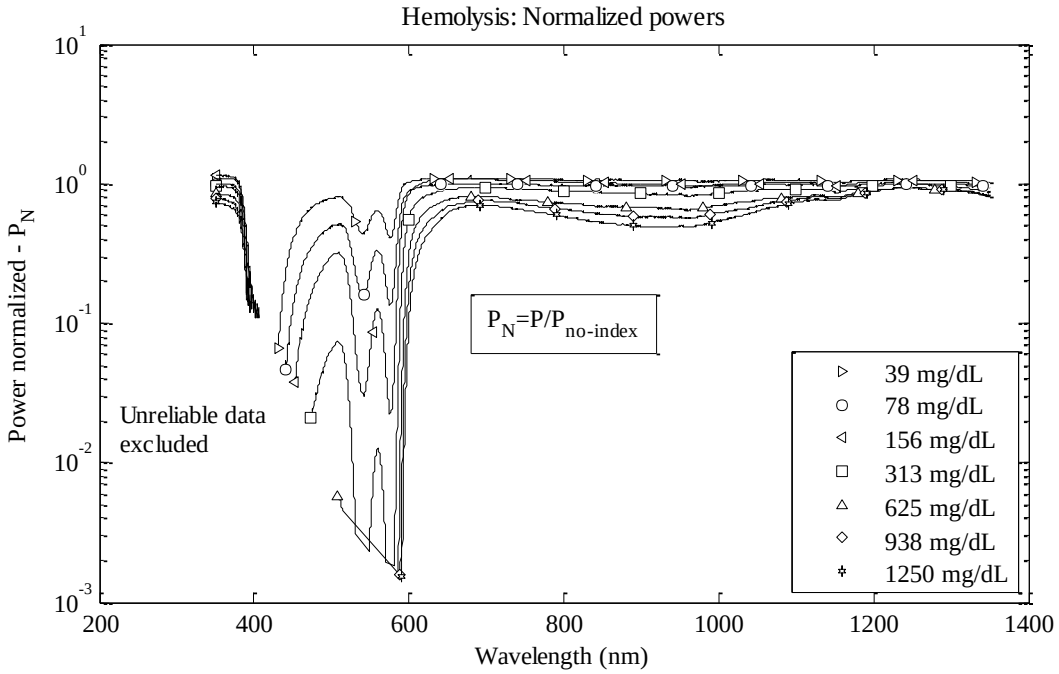

Figure 3.6 Power normalized for Hemolysis samples with power through no-index serum

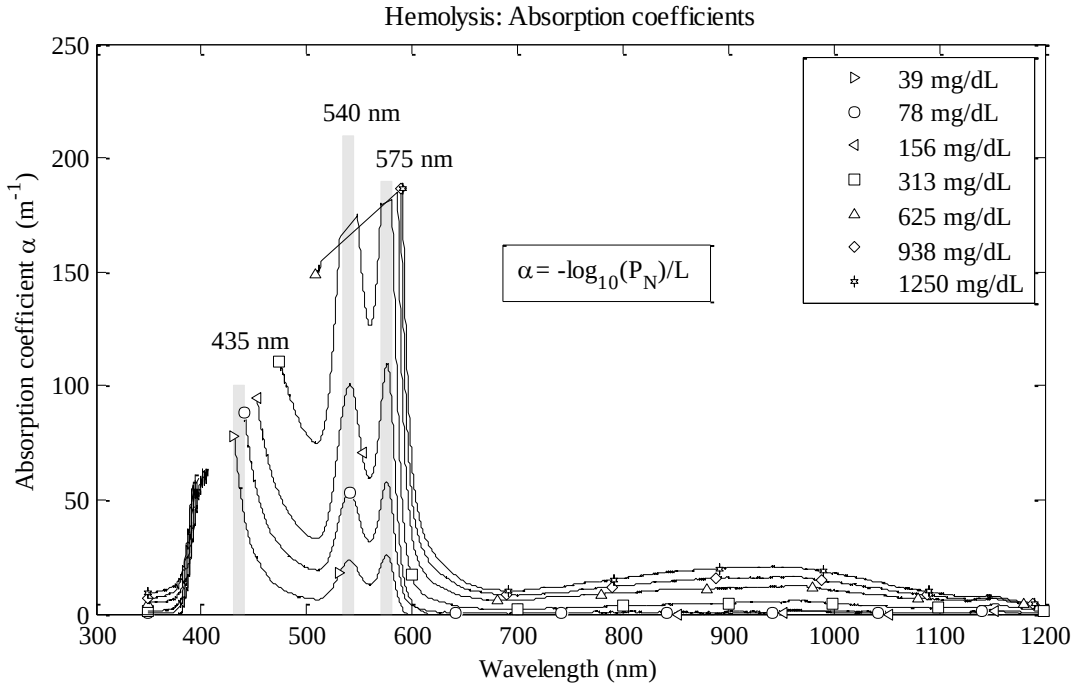

Figure 3.7 Absorption coefficients of Hemolysis.

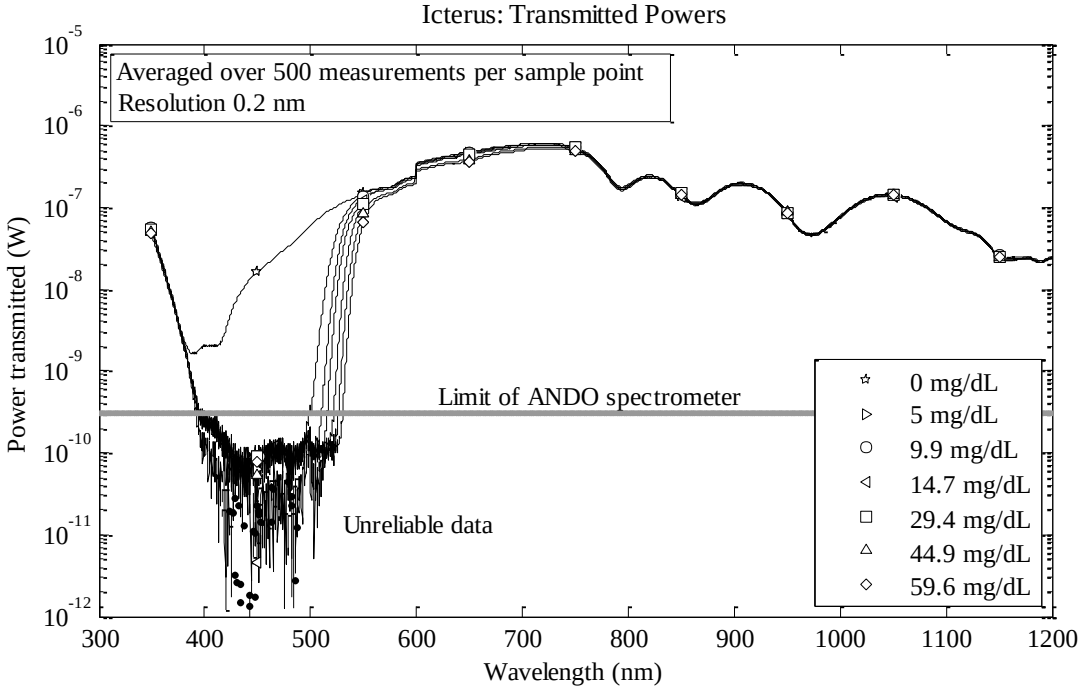

Figure 3.8 Power transmitted through serum samples with Icterus

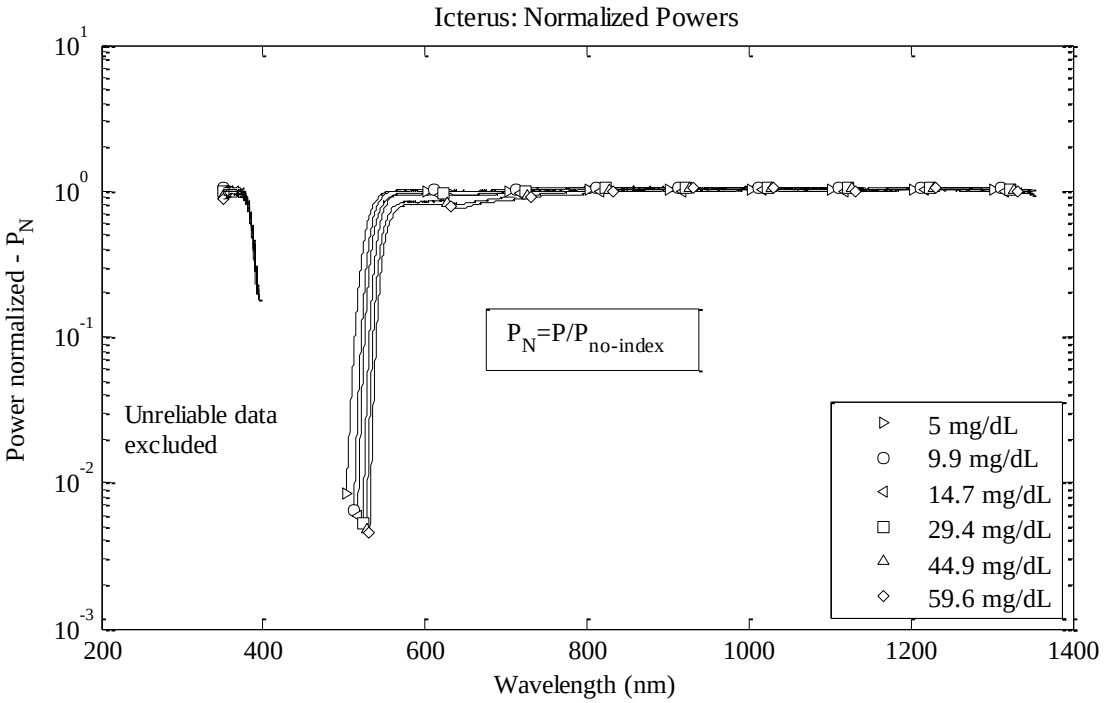

Figure 3.9 Power normalized for Icterus samples with power through no-index serum.

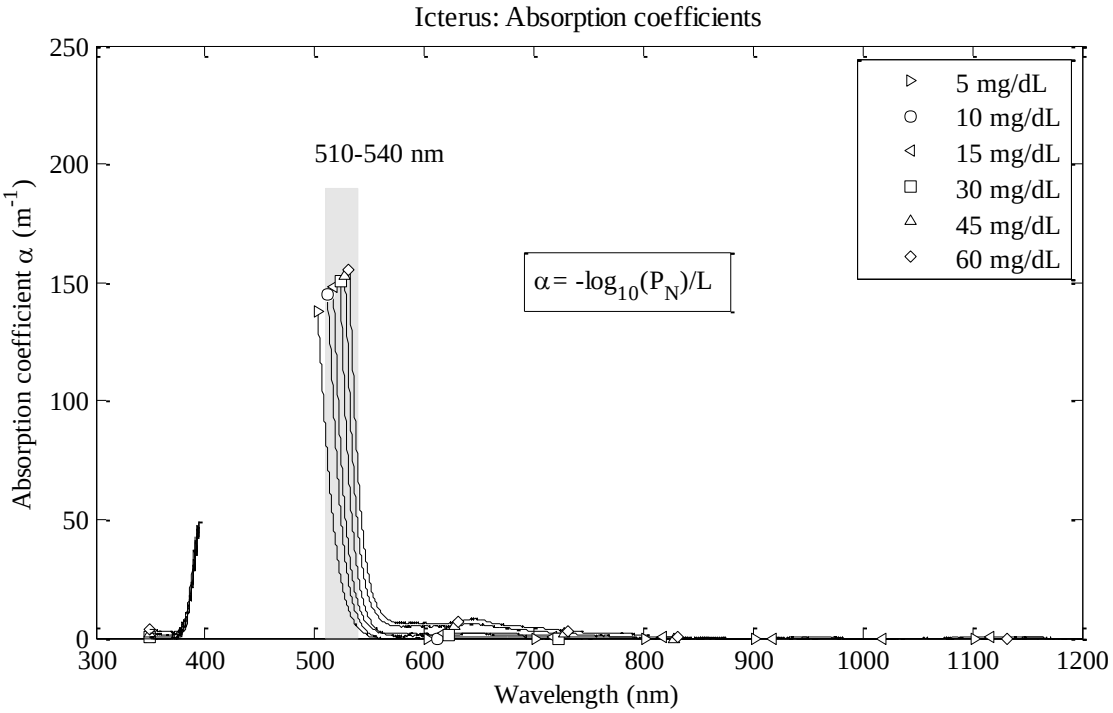

Figure 3.10 Absorption coefficients of Icterus.

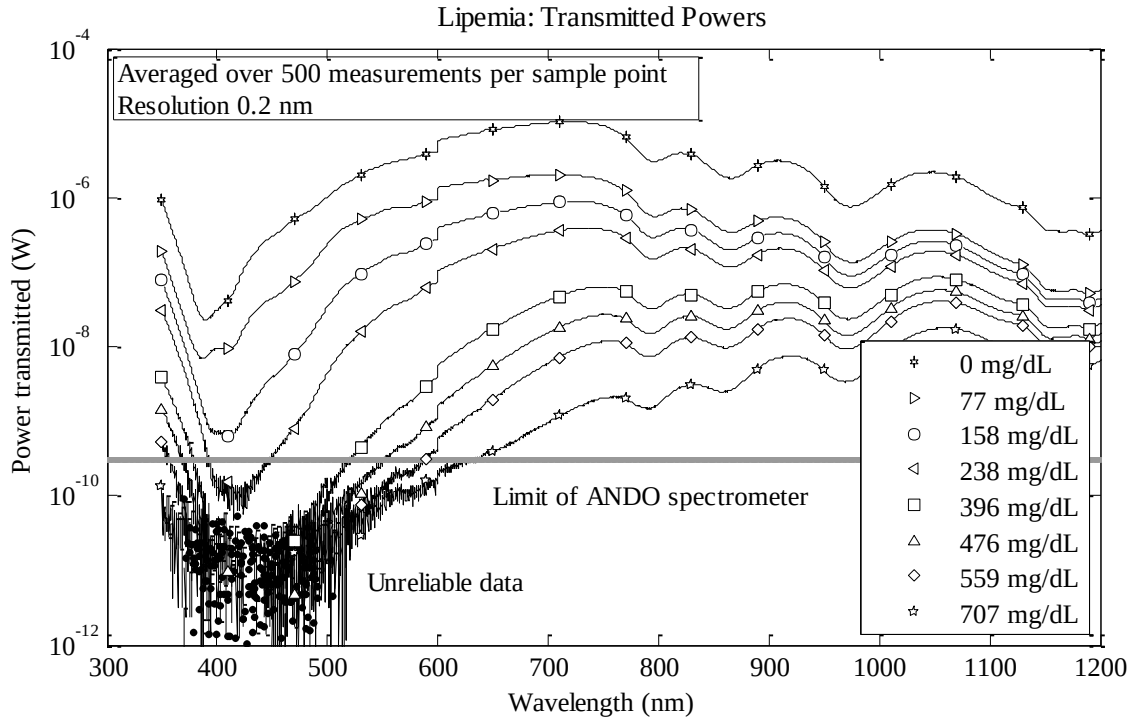

Figure 3.11 Power transmitted through serum samples with Lipemia.

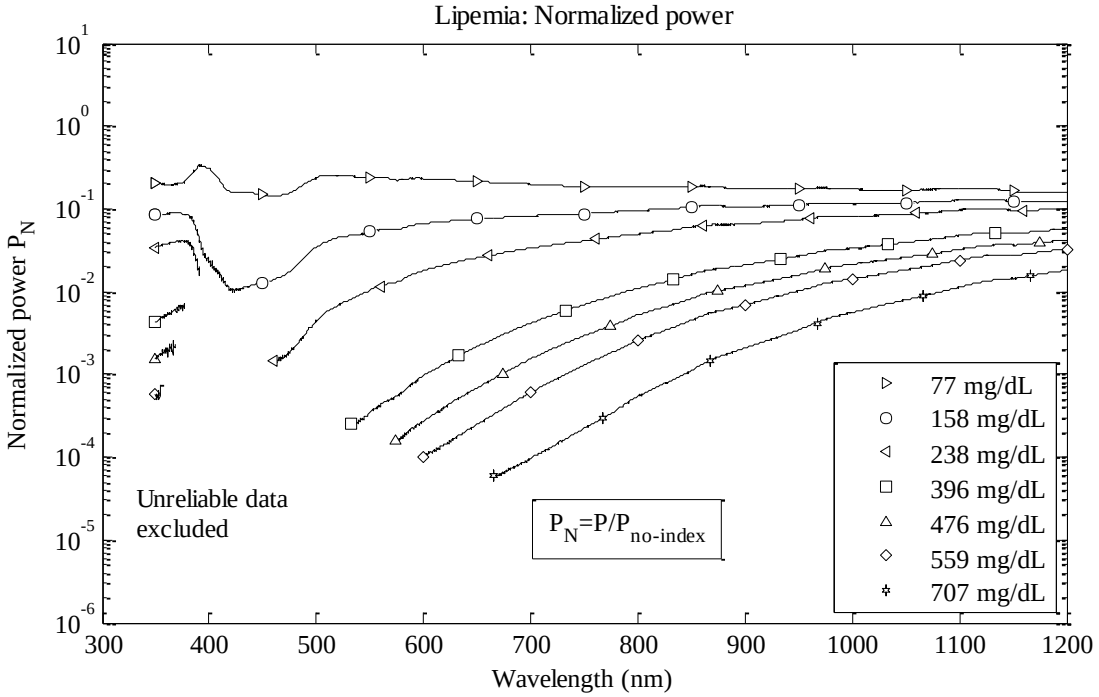

Figure 3.12 Power normalized for Lipemia sample with power through no-index serum.

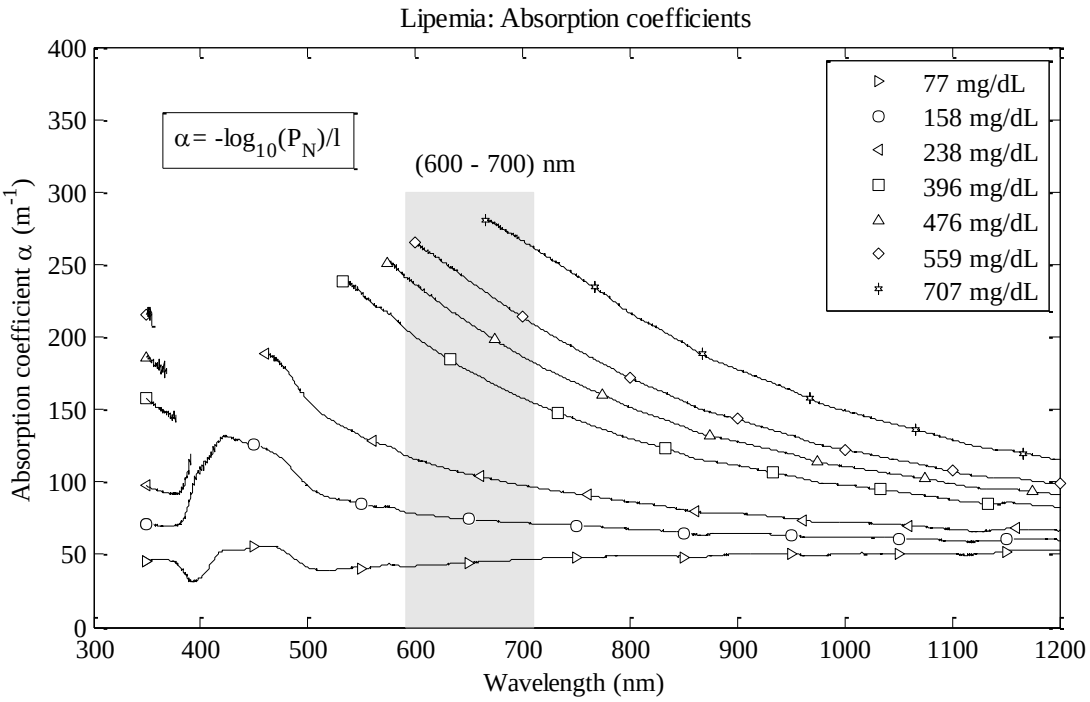

Figure 3.13 Absorption coefficients of Lipemia

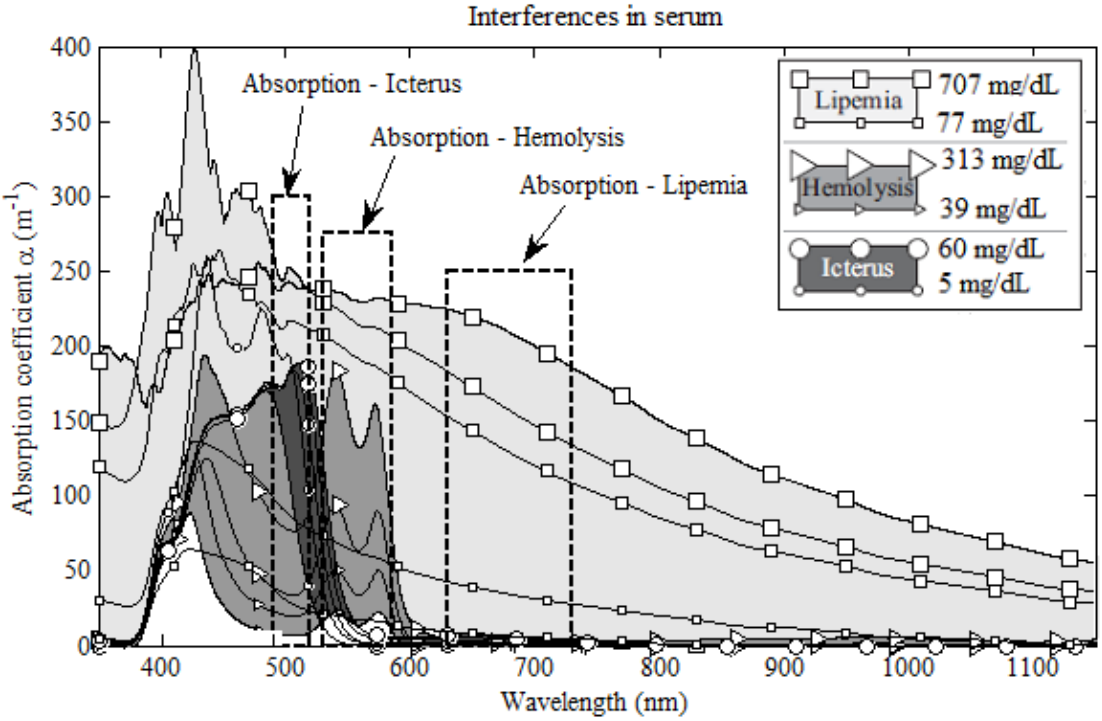

Figure 3.14 Combined absorption coefficients of Hemolysis, Icterus, and Lipemia

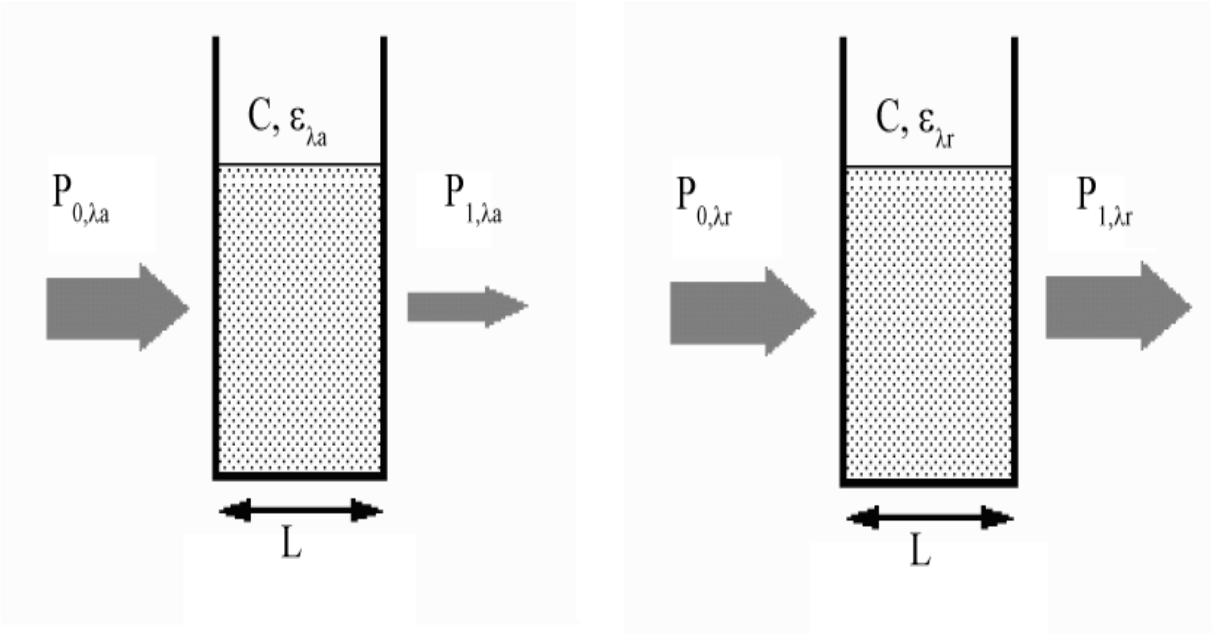

Figure 3.15 Principle of quantification of interferences

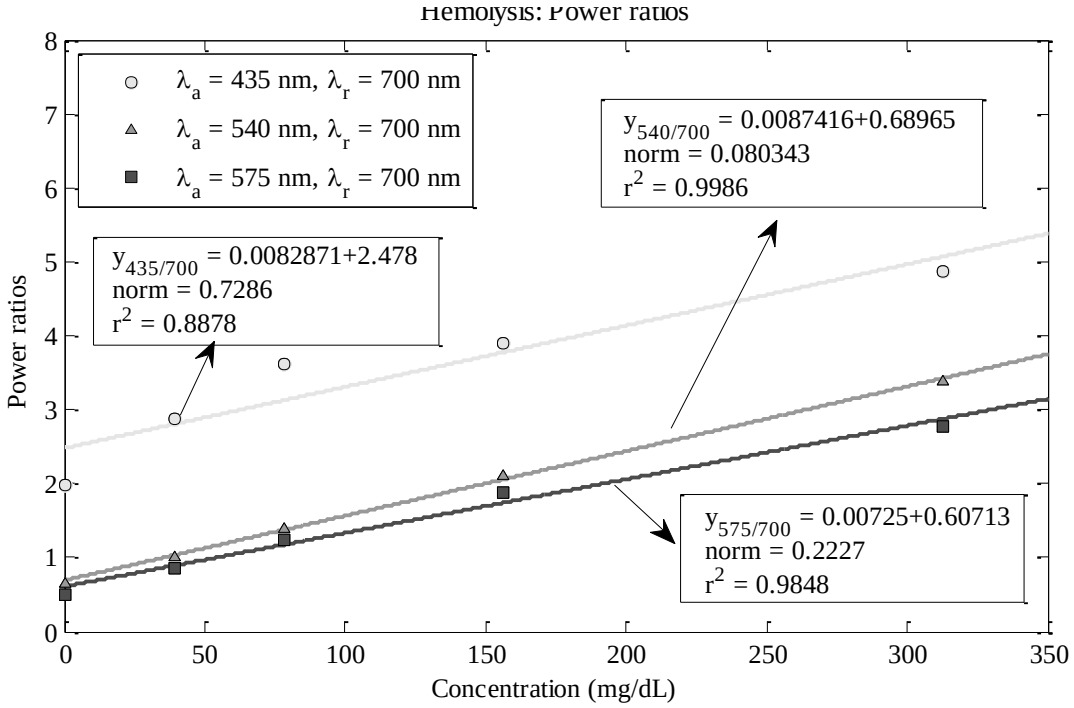

Figure 3.16 Linearity between power ratios and concentrations for Hemolysis

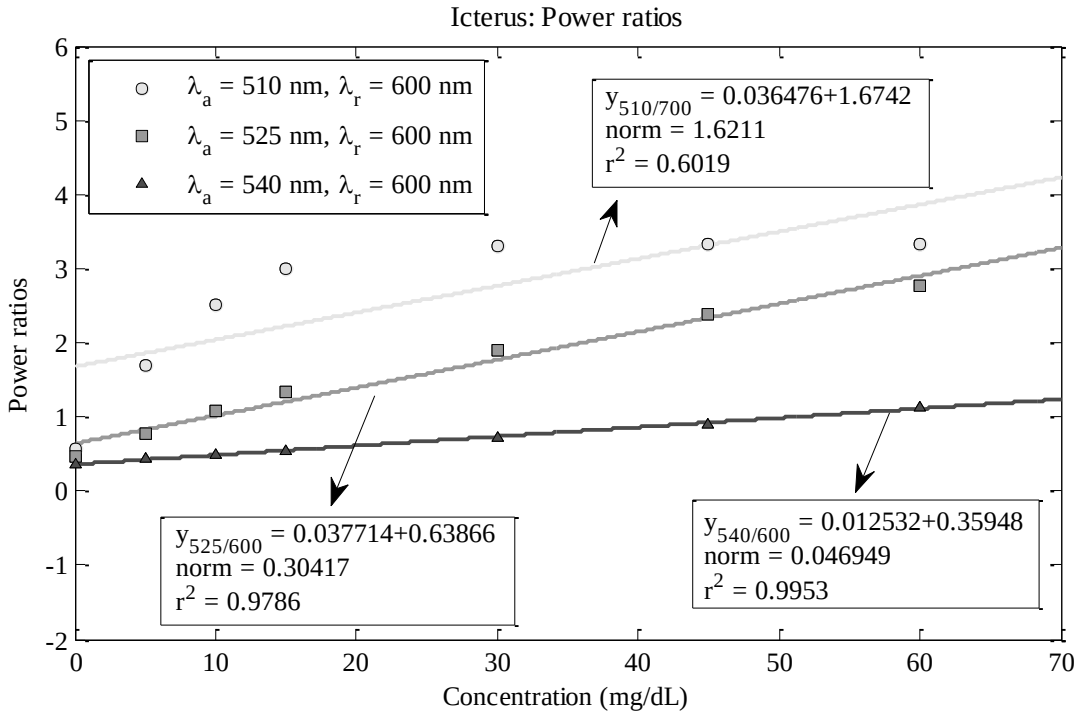

Figure 3.17 Linearity between power ratios and concentrations for Icterus

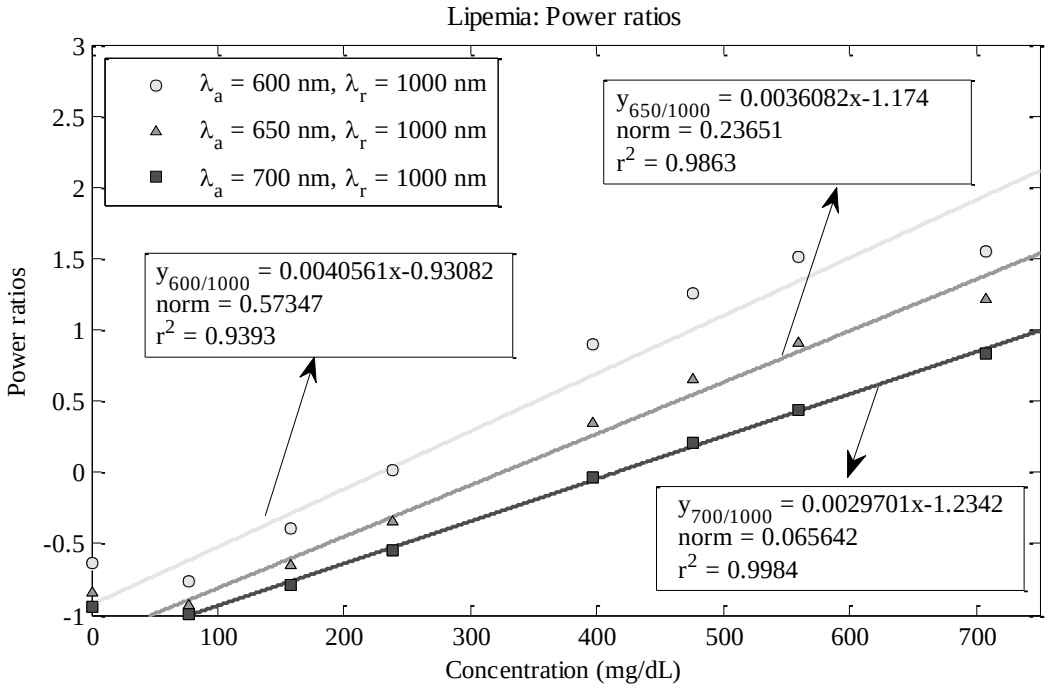

Figure 3.18 Linearity between power ratios and concentrations for Lipemia

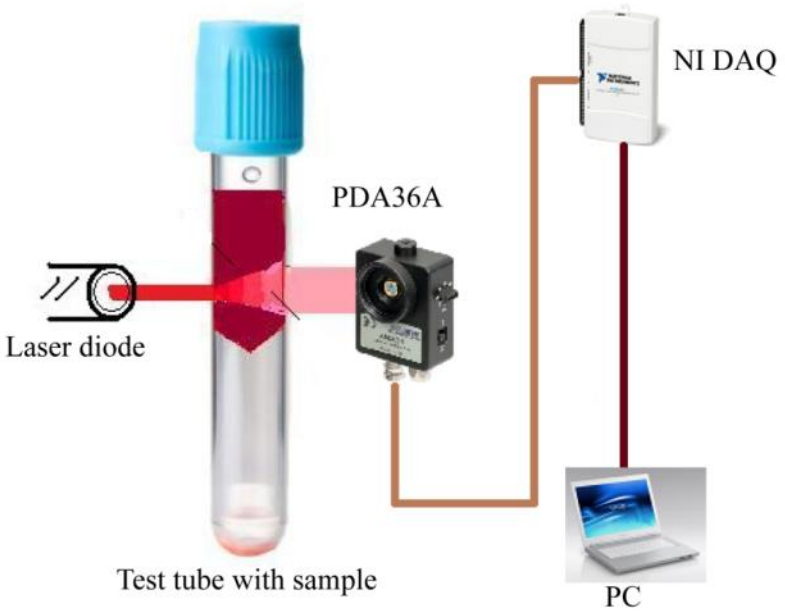

Figure 3.19 Schematic of the experimental set-up

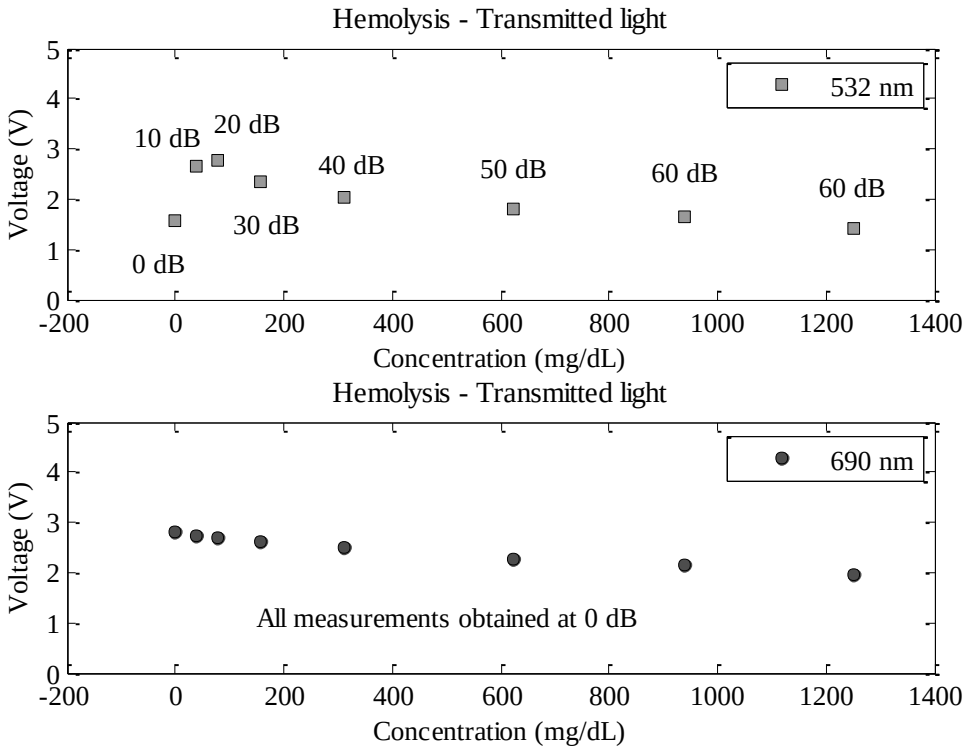

Figure 3.20 Transmitted light for Hemolysis as voltage signals at different gain levels.

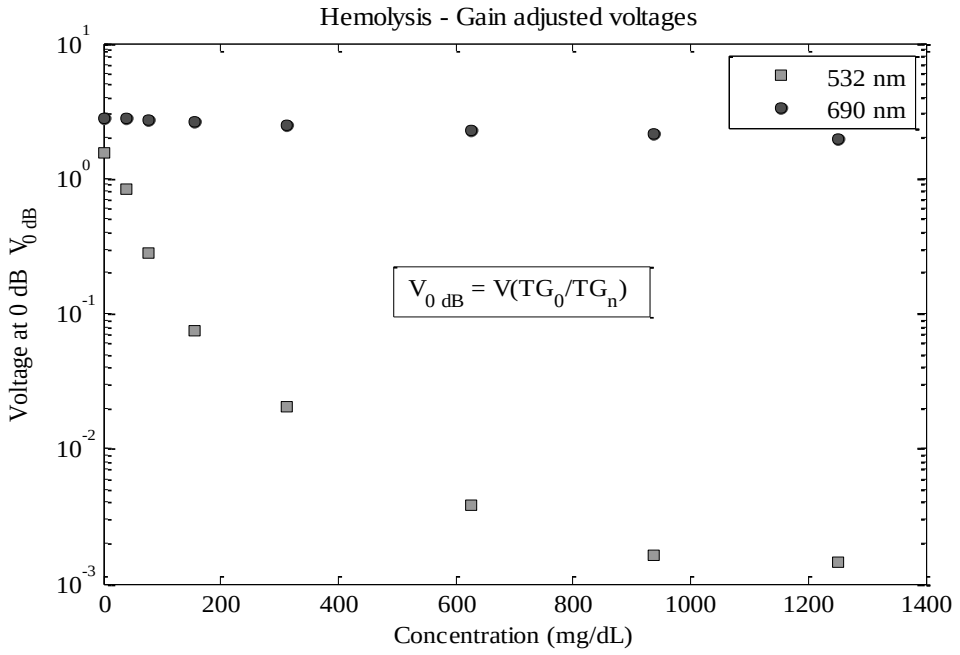

Figure 3.21 Gain adjusted voltage values for Hemolysis

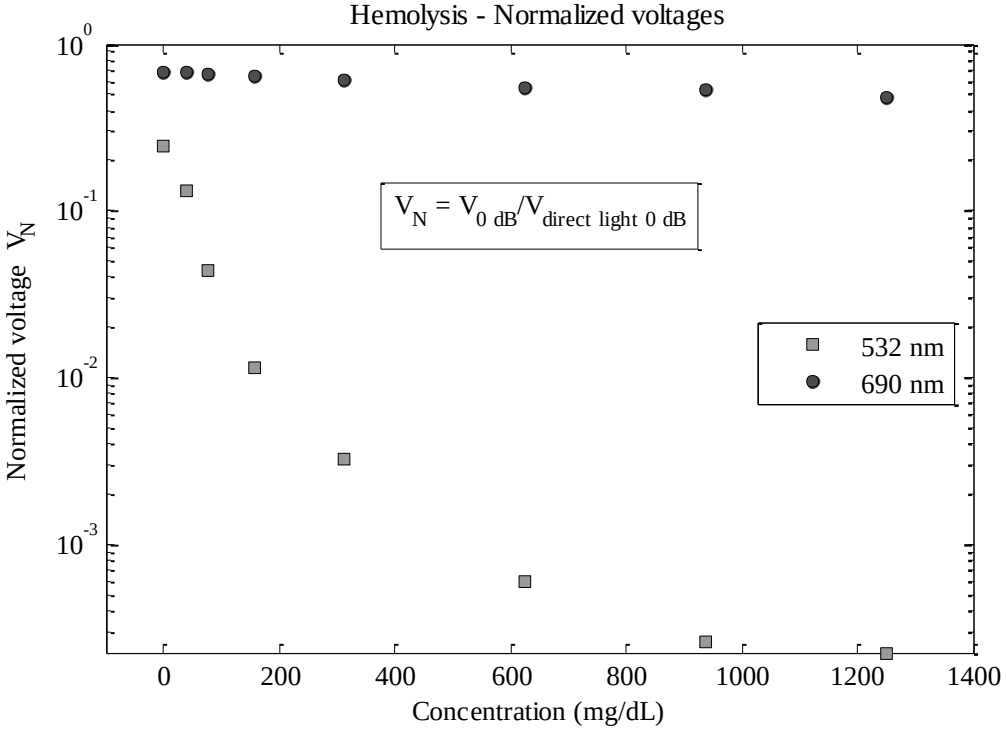

Figure 3.22 Normalized voltage values for Hemolysis

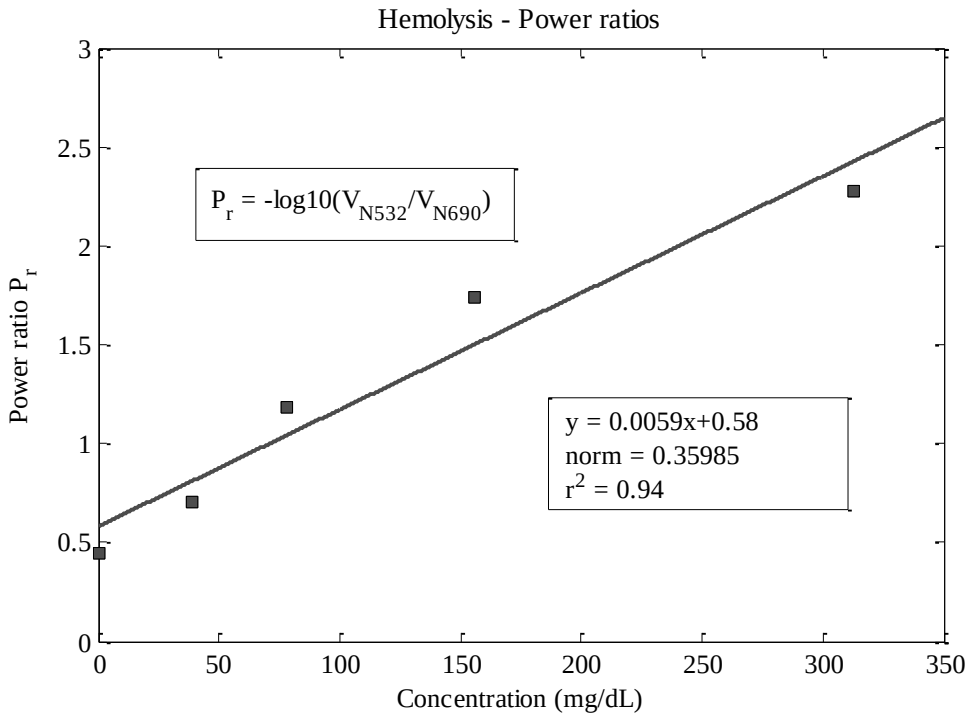

Figure 3.23 Linearity between power ratios and concentration for Hemolysis

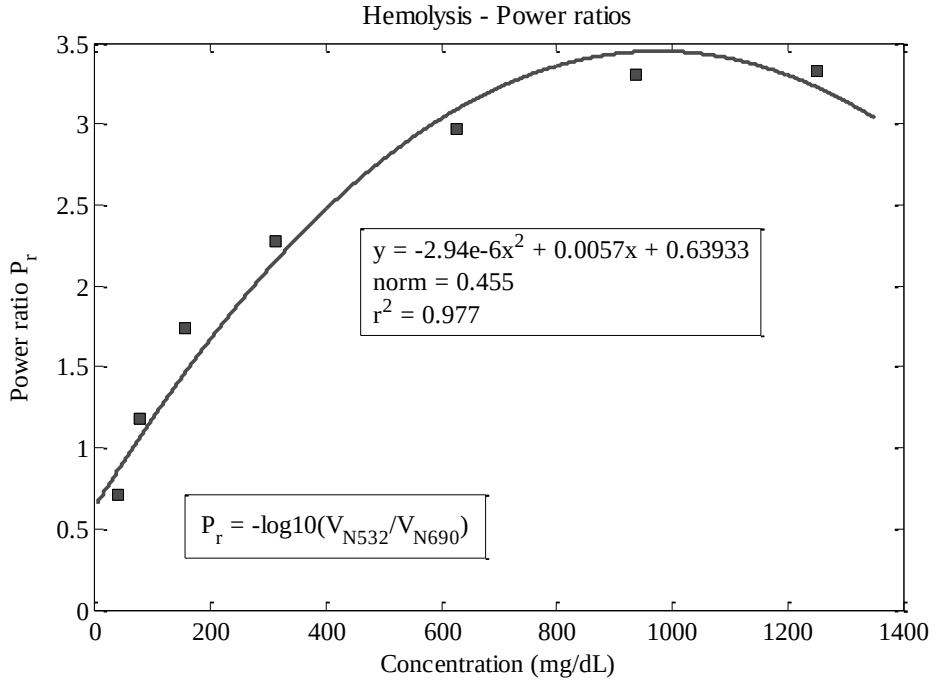

Figure 3.24 Polynomial fit between power ratios and concentration for Hemolysis

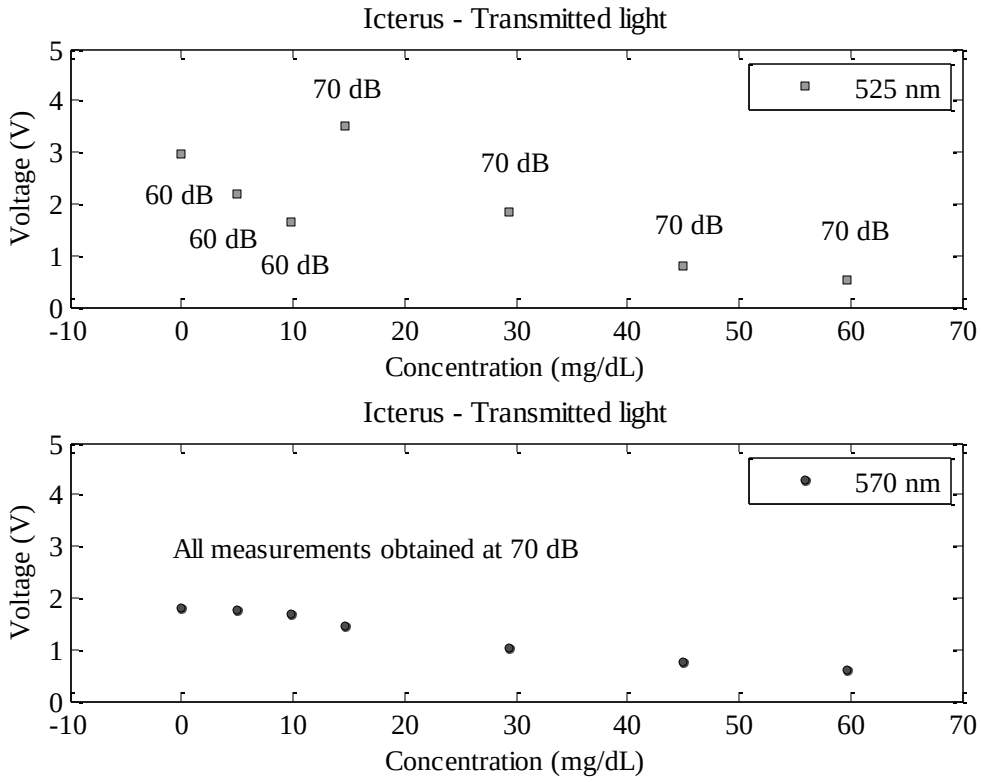

Figure 3.25 Transmitted light for Icterus in terms of voltage signals at different gain levels

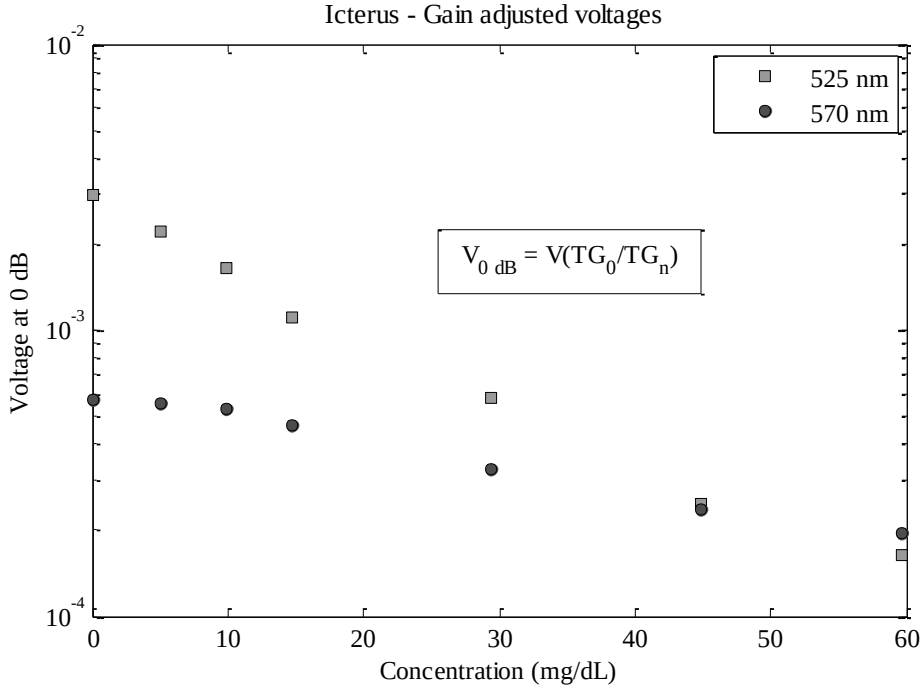

Figure 3.26 Gain adjusted voltage values for Icterus

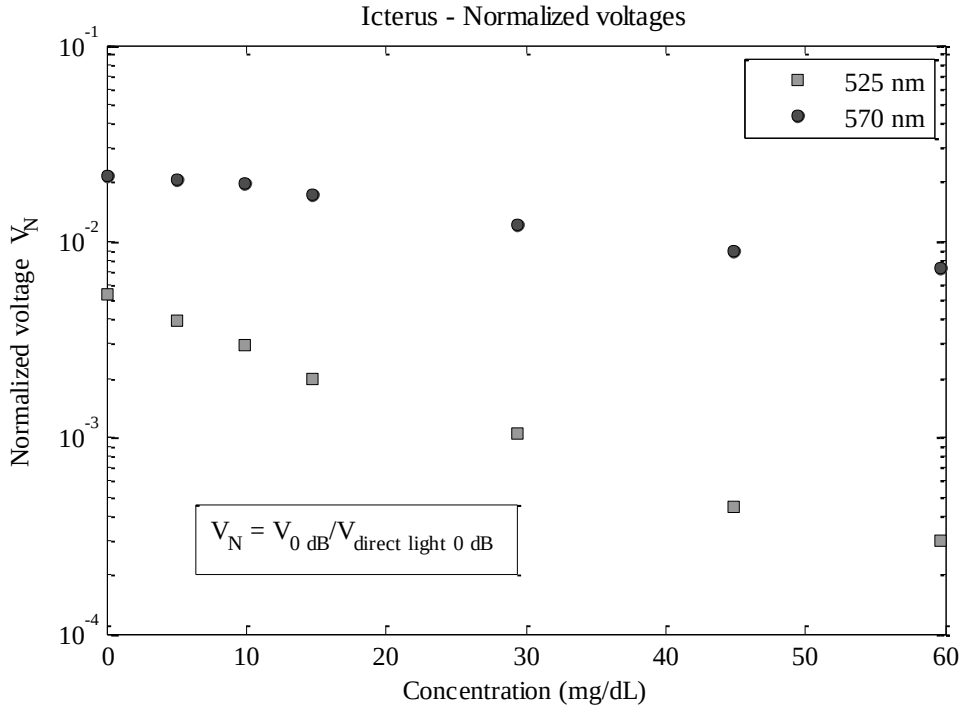

Figure 3.27 Normalized voltage values for Icterus

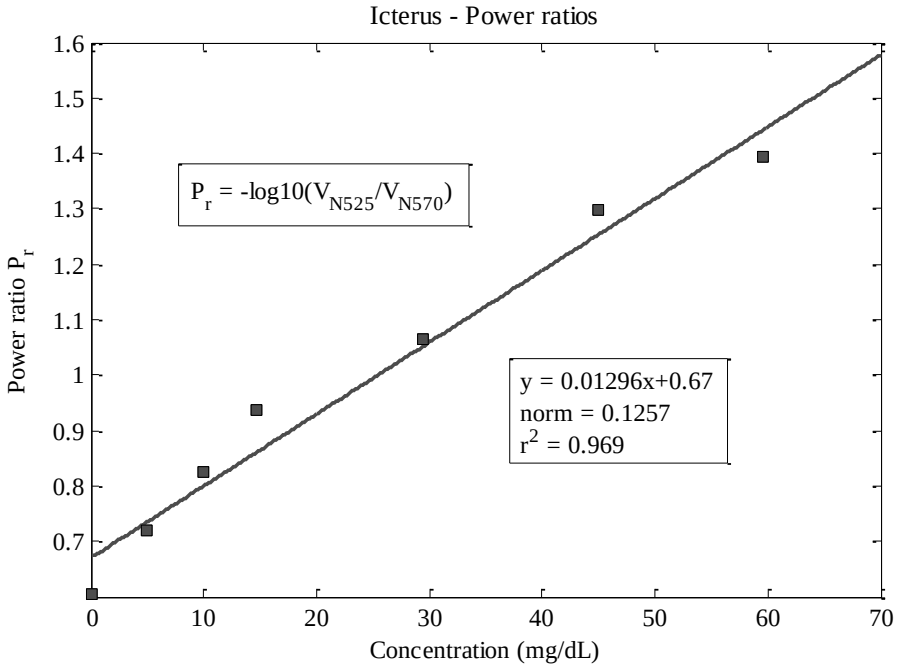

Figure 3.28 Linearity between power ratios and concentration for Icterus

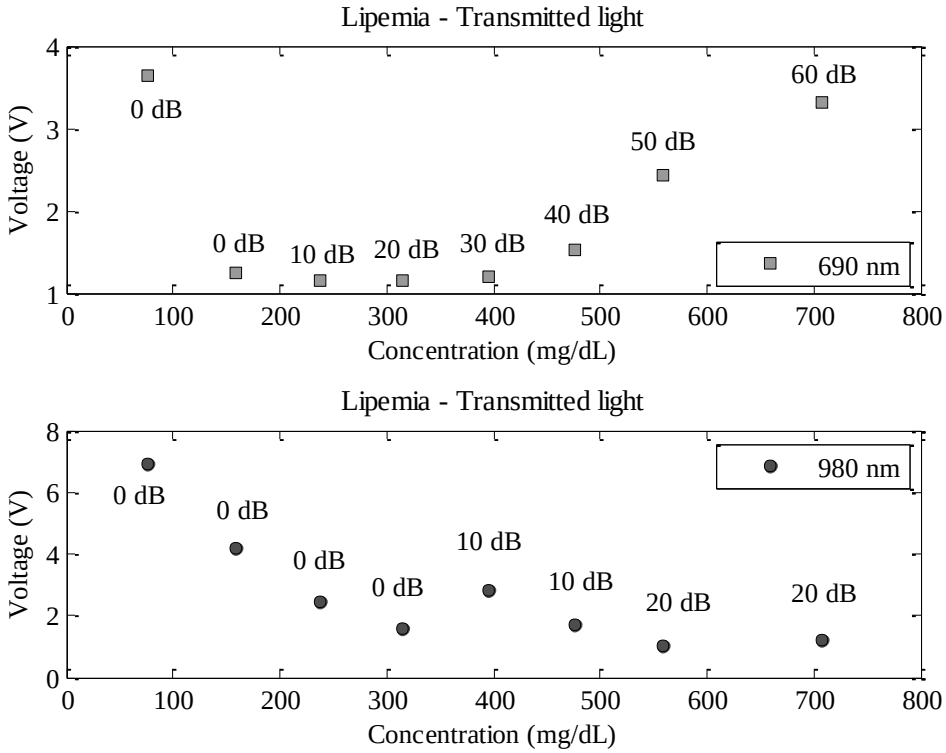

Figure 3.29 Transmitted light for Lipemia as voltage signals at different gain levels

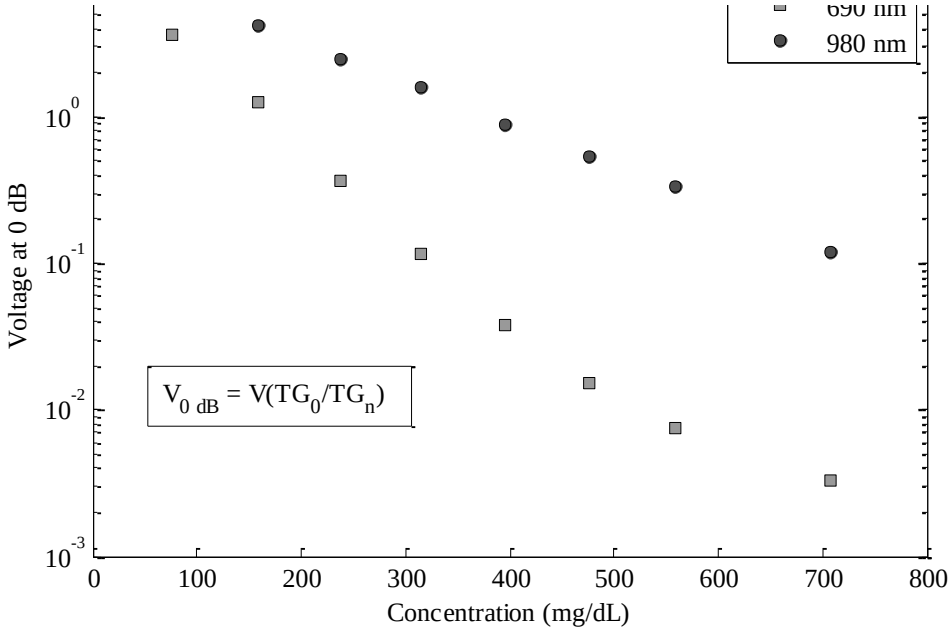

Figure 3.30 Gain adjusted voltage values for Lipemia

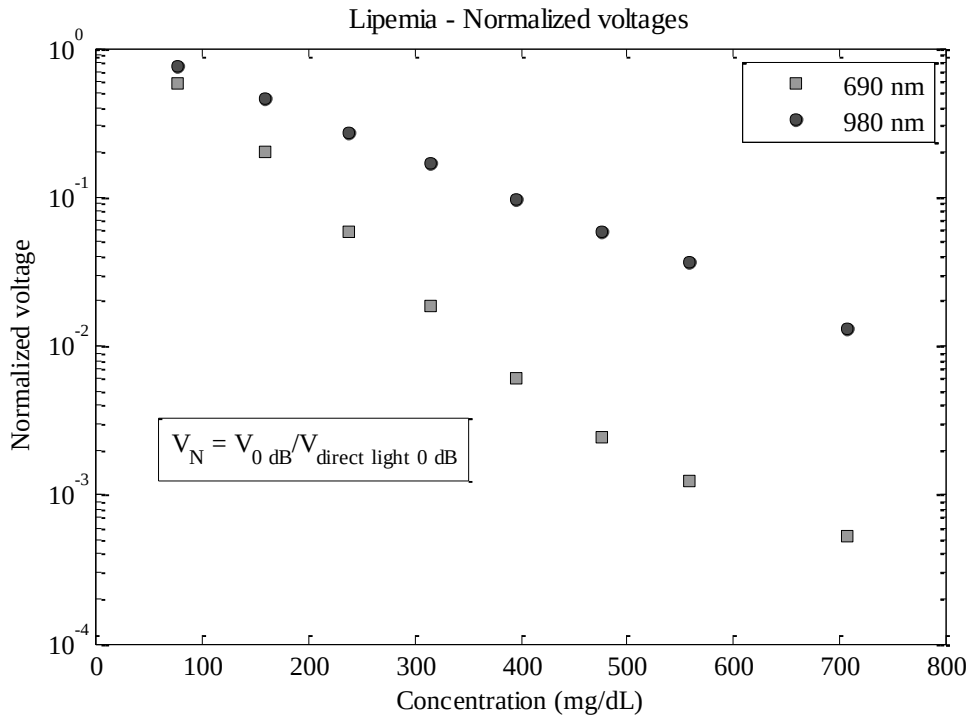

Figure 3.31 Normalized voltage values for Lipemia

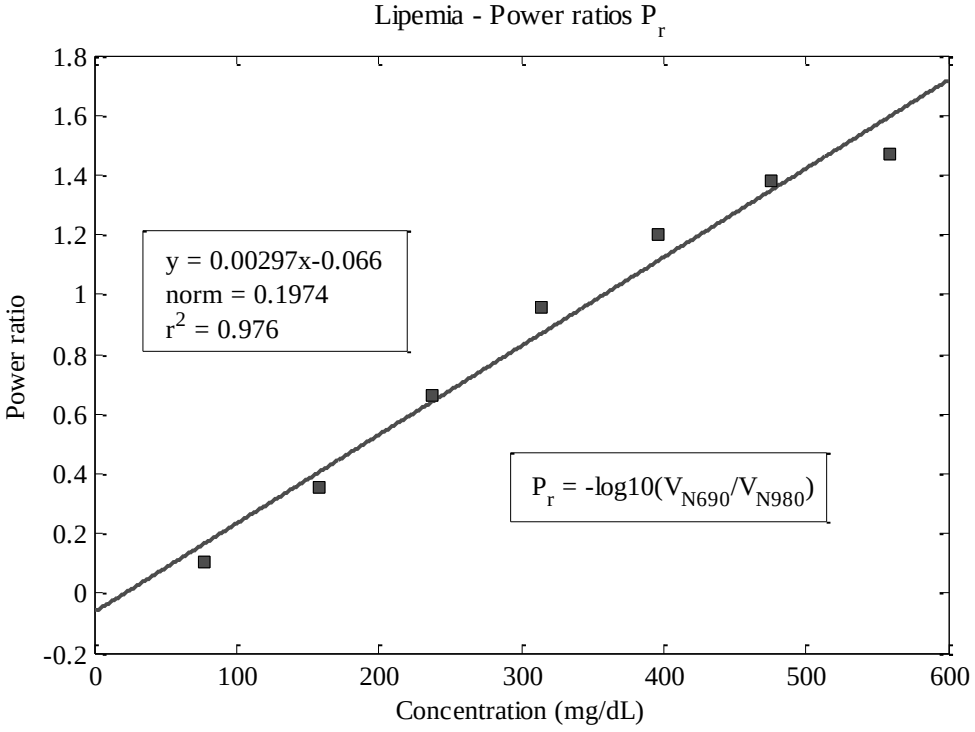

Figure 3.32 Linearity between power ratios and concentration for Lipemia

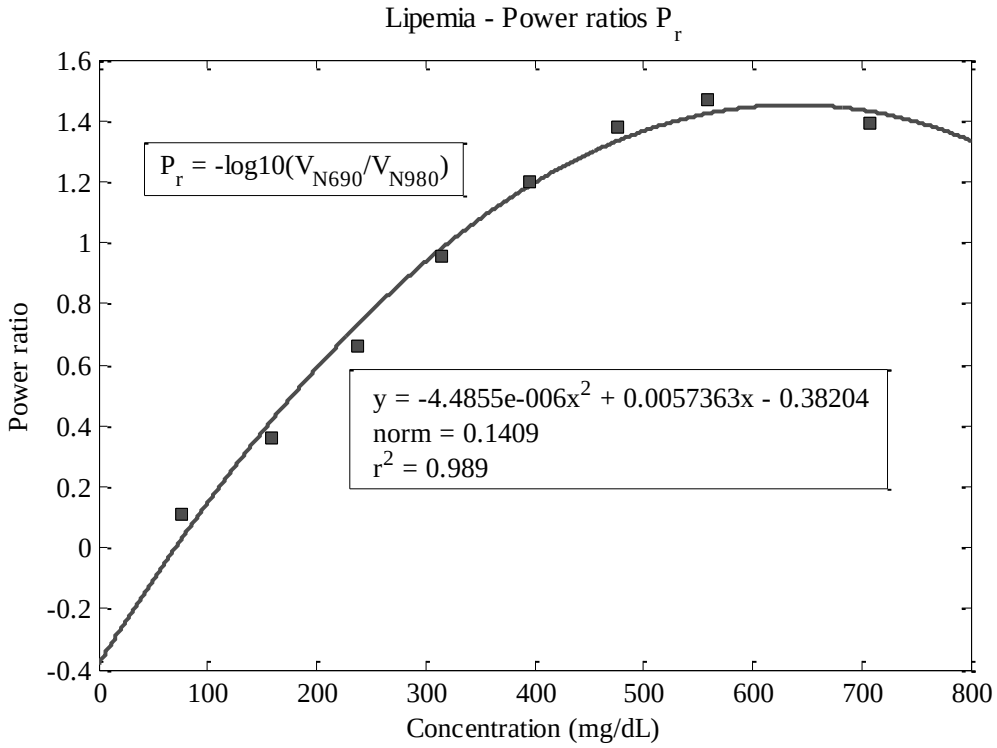

Figure 3.33 Polynomial fit between power ratios and concentration for Lipemia

CHAPTER 4

RADIATIVE HEAT TRANSFER MODEL

4.1 Introduction

The selection of the light sources (LDs and LEDs) used in the experiment described in section 3.6 was based on the wavelength requirements as per the principle of detection, but did not include the requirements of optical output power. When labels were attached on the outside of the tube, the transmitted power was too low. For example, for a test tube containing serum sample with Hemolysis and covered with a combination of 3 labels (2 on one side and one on the other side) attached on the outside, when tested with the 532 nm LD, the measured voltage using the photo detector was 0.05 V at 70 dB (maximum gain level). The maximum offset of the detector (PDA36A) at 70 dB is 200 mV, meaning that even without any light, the detector may show a reading of up to 0.2 V and hence, the readings are unreliable. Thus, the system requires higher power light sources but high-power lasers might cause an increase in the temperature of the biological samples. Most of the tests that are being conducted in the core laboratory of ARUP Labs require maintaining the test specimens at room temperature [1]. The radiant power of light transmitted and the thermal effect on the biological specimen can be used in the selection of light sources. In order to model the radiant power of transmitted light, the temperature distribution in a sample, and to understand the effects of spectral radiative properties like absorption and scattering for a liquid sample in a tube irradiated by means of a laser light,

a radiative heat transfer model was formulated using a commercially available CFD software package FLUENT. This chapter explains the radiative transfer theory involved, the implementation of radiative transfer in participating media, the parameters and settings used in the FLUENT model like material properties, boundary conditions, etc., and the results obtained are discussed in the final sections.

4.2 Model Formulation

The radiative heat transfer or thermal radiation is the science of heat transfer caused by electromagnetic waves. The current problem consists of a liquid sample in a test tube irradiated by a laser beam. LASER (Light Amplification by Stimulated Emission of Radiation) is a light source that emits electromagnetic radiation through optical amplification based on the stimulated emission of photons. Each of the electromagnetic waves or the photons carry with them an amount of energy, E = hν (h, Planck's constant $= 6.626 * 10^{-34}$Js, ν = frequency). When an electromagnetic wave propagates through a medium, its energy may continuously attenuate. If the wave passes through an opaque medium, the attenuation is complete and there is no radiation emerging; if the wave travels through a transparent medium, there is no attenuation. When it passes through a semitransparent medium, there is partial attenuation. The characterizing of these media depends on the material properties and the thickness of the medium [22]. Serum is a semitransparent liquid or an absorbing, emitting, and scattering medium so the radiative transfer through participating media must be accounted for.

4.2.1 Radiative Transfer in Participating Media

In a participating medium, an incident light beam in the direction $\vec{s}$ loses energy by absorption and out scattering (scattering away from the direction of travel) and at the

same time gains energy by emission and in-scattering (scattering from other directions into the direction of travel, $\vec{s}$) [22], as described in Figure 4.1. The radiative transfer equation (RTE) for a gray (independent of wavelength), absorbing, emitting, and scattering medium at position $\vec{r}$ in the direction $\vec{s}$ is [23]

$$\nabla.(I(\vec{r},\vec{s})\vec{s}) + (a+\sigma_s)I(\vec{r},\vec{s}) = an^2\frac{\sigma T^4}{\pi} + \frac{\sigma_s}{4\pi}\int_0^{4\pi} I(\vec{r},\grave{\vec{s}})\Phi(\vec{s}.\grave{\vec{s}})\,d\grave{\Omega} \qquad (4.1)$$

where $\vec{r}$ = position vector

$\vec{s}$ = direction vector

$\grave{\vec{s}}$ = scattering direction vector

s = path length

a = absorption coefficient

n = refractive index

σ_s= scattering coefficient

σ = Stefan-Boltzmann constant (5.67x10e^{-8} W/m^2K^4)

I = radiation intensity (depends on position r and direction s)

T = local temperature

Φ = phase function

$\grave{\Omega}$ = solid angle

The total attenuation by absorption and scattering is known as the extinction, β (=a+σ_s) and the optical thickness or opacity of a medium is defined as the product of extinction coefficient with the thickness or the path length (a+σ_s)s.

4.2.2 Numerical Methods

The radiation intensity is a function of position, direction, and wavelength which makes thermal radiation a complex phenomenon to analyze. Various numerical methods were developed to solve the radiative transfer equation, of which the important ones are Monte Carlo Method, Radiation Element Method, Flux Method, Discrete Transfer Method, Spherical Harmonics Method, Finite Volume Method, and Discrete Ordinates Method [22].

With the handiness of modern high-performance computing capabilities and development of user-friendly interfaces, several free and commercial CFD packages have been developed. COMSOL Multiphysics, CFX, FLOW 3D, and ANSYS FLUENT are a few to mention. In the present work, ANSYS FLUENT is used in modeling radiative heat transfer in participating media. FLUENT is engineering simulation software with broad modeling capabilities needed to model fluid flow, heat transfer, and chemical reactions in complex geometries. It is written in C computer language and so offers true dynamic memory allocation, efficient data structures, and flexible solver control. Unstructured meshes generated in complex geometries can be handled with ease through complete mesh flexibility in FLUENT [23].

4.2.3 Discrete Ordinates Method and Its Implementation in FLUENT

There are 5 different models available in ANSYS FLUENT by means of which the radiation can be included in hear transfer calculations. They are:

1. Discrete Transfer Radiation Model (DTRM)
2. P-1 Radiation Model
3. Rosseland Radiation Model

4. Surface to Surface Radiation Model (S2S)
5. Discrete Ordinates Radiation Model (DO)

The Discrete Ordinates Radiation Model was selected for the current problem based on the following advantages:

a. It allows including absorption, scattering, and particulate effects in semi-transparent media and allows radiation calculations at semitransparent walls.
b. It allows solving problems that span an entire range of optical thickness; the tube and the liquid elements have different optical thicknesses at different wavelengths.
c. Non-gray (wavelength dependent) implementation is possible in addition to the gray implementation and is intended for use with a participating medium with a spectral absorption coefficient.
d. The memory requirements and computational costs are moderate for typical angular discretization.

The method of discrete ordinates involves finite differencing of the directional variation of the radiative intensity. It solves the RTE for a finite number of solid angles, each associated with a direction vector $\vec{s}$ fixed in the global Cartesian system. In the DO model, equation (4.1) is transformed into a transport equation for radiation intensity in spatial coordinates and solves for as many transport equations as there are directions ($\vec{s}$**).**

Equation (4.1) holds good for a gray participating media whose radiative properties like absorption coefficient, scattering coefficient, and phase function do not vary across the electromagnetic spectrum, which is unlikely to happen in liquids like water and serum. The variation of the absorption coefficient of water with wavelengths in UV,

Visible, and IR spectrum is shown in the Figure 4.2. This is because the internal molecular energy of semitransparent media like gases and liquids consists of contributions from electronic, vibration, and rotation energy states. So when light passes through these media, the molecule may absorb a passing photon raising one of the internal energy states, or it may emit a photon to lower one of its internal energy states.

4.2.4 Non-gray Implementation of DO model

In previous experiments, laser diodes of wavelengths 532 nm, 690 nm, and 980 nm were used for the monochromatic irradiation of the samples. In order to calculate the spectral intensity using the DO model in FLUENT, the non-gray radiation is modeled using a gray band model. The RTE for spectral intensity I_λ is written as [23]

$$\nabla.(I_\lambda(\vec{r},\vec{s})\vec{s}) + (a_\lambda + \sigma_s)I_\lambda(\vec{r},\vec{s}) = a_\lambda n^2 I_{b\lambda} + \frac{\sigma_s}{4\pi}\int_0^{4\pi} I_\lambda(\vec{r},\vec{\hat{s}})\Phi(\vec{s}.\vec{\hat{s}})\, d\hat{\Omega} \qquad (4.2)$$

where λ is the wavelength of light used, a_λ is the spectral absorption coefficient, and $I_{b\lambda}$ is the blackbody intensity given by Planck function. The remaining factors like scattering coefficient, scattering phase function, and the refractive index n are assumed independent of wavelength λ. In the non-gray DO implementation, the radiation spectrum is divided into N wavelength bands, and the blackbody emission in the wavelength band per unit solid angle is written as

$$\{F(0 \to n\lambda_2 T) - F(0 \to n\lambda_1 T)\}n^2 \frac{\sigma T^4}{\pi}$$

where $F(0 \to n\lambda T)$ is the fraction of energy emitted by blackbody in the wavelength interval from 0 to λ at temperature T in a medium of refractive index n. Within each band, the behavior of the medium is assumed to be gray.

4.2.5 Overall Energy Conservation

Thermal radiation is just one of the modes of heat transfer and must compete with the other modes of heat transfer like conduction and convection. The temperature field is calculated through an energy conservation equation that incorporates all possible modes of heat transfer. The radiation intensity cannot be decoupled from the energy equation as it depends on the temperature field. So when the DO Radiation Model is activated in FLUENT, the energy equation is automatically enabled. A general form of energy equation can be written as [22]

$$\rho C_v \left(\frac{DT}{Dt}\right) = \nabla.(k\nabla T) - p\nabla.v + \mu\varphi + \dot{Q}''' - \nabla.q_R \qquad (4.3)$$

where $k\nabla T$, the conductive heat flux, is vector and q_R represents the radiative heat flux. The second term on the right-hand side represents the flow and is equal to zero as there is no flow in this case. Third and fourth terms represent viscous dissipation and volumetric heat generation, respectively, which are not applicable for the present case.

4.2.6 Coupled and Uncoupled Variations of DO Model

The DO Radiation Model can be implemented in two variations, namely uncoupled and (energy) coupled. The uncoupled implementation is sequential in nature and uses finite-volume scheme to solve the equations for the energy and radiation intensities one by one, assuming prevailing values for other variables. In the coupled method, the discrete energy and radiation intensities are solved simultaneously assuming spatial neighbors are known. This method can be used for applications involving high opacity or for applications containing high scattering coefficients because the simultaneous solving of equations makes it possible to achieve the convergence faster. In the current model, the

uncoupled implementation is used as the optical thicknesses are comparatively smaller (explained in section 4.3.3).

4.3 Model Settings

The following section describes the settings and parameters used in the model and the assumptions used in modeling.

4.3.1 Geometry and Mesh Generation

The geometry was developed in GAMBIT, a software package designed for building geometries and meshing them for computational fluid dynamics and other scientific applications. The GAMBIT GUI makes the basic steps of building, meshing, and assigning boundary types and zone types simple and intuitive.

For simplification, the geometry was approximated by a cylindrical volume element of 3 ml. The volume element is drawn by stitching circular and cylindrical faces. Initially, only a single volume representing the fluid zone was drawn; later, two concentric volumes representing the fluid and solid zones were drawn, as shown in Figure 4.3. Wall 1, Wall 2, Wall 3, Wall 4, and Wall 5 enclose the solid zone and Wall 6, Wall 7, Wall 8, and their respective shadow walls separate the liquid zone from the solid zone. The shadow walls are a result of subtraction of volumes to create the two zones. Different laser diodes result in different beam widths and shapes; for a generic model, the beam that is incident on the tube wall was approximated to a circular beam of diameter 2 mm, so a face (Wall 1) with 2 mm diameter was drawn on the cylindrical face. To consider the detector on which the transmitted light is detected a face (Wall 2) of diameter equal to the diameter of the photodiode was drawn on the cylindrical face.

The geometry was fine meshed with a default tetrahedral scheme of tet/hybrid elements to result in 181712 elements in the fluid zone and 75020 elements in the solid zone volume. Figure 4.4 shows the meshed geometry. Boundary types for all the faces were assigned as walls and continuum zones were assigned to the volume elements as solid and fluid zones. Finally, the mesh was exported to FLUENT 6.

4.3.2 Model Definition

First, the 3D mesh file was imported into FLUENT and the grid was verified and scaled to the appropriate units (m). The DO Radiation Model was activated with 1 spectral band with the wavelength of the laser used as described in non-gray implementation (section 4.2.4). The angular discretization was given as $N_\theta x N_\varphi = 10x10$. These divisions will define the number of control angles used to discretize each octant of angular space, so for a 3D model, a total of $8N_\theta N_\varphi$ directions are solved. Initially, lower values were tried, and to improve the accuracy in the cylindrical geometry where specular exchange of radiation is important, higher order discretization was used. The computational effort increases with the number of divisions.

4.3.3 Material Properties

Instead of serum samples with interferences like Hemolysis, Lipemia, Icterus, etc. water was used as the liquid zone in modeling as per the availability of thermal and radiative properties in FLUENT database. Polypropylene which is the tube material was used for the solid zone. Scattering was assumed negligible for water and polypropylene. Radiative properties like refractive index and absorption coefficient were provided for radiation calculations. Table 4.1 shows the values of absorption coefficients of water and

tube obtained from the literature and the respective optical thickness or opacity values are calculated.

4.3.4 Boundary Conditions

Cell zone conditions were provided to liquid and solid zones as stationary and participating in radiation. Two categories of boundary conditions were provided at the walls - thermal boundary conditions applied for heat transfer calculations and radiation boundary conditions for calculations using the DO model.

The model contains exterior walls that enclose the solid zone and the interior walls that separate the liquid and solid zone. All the walls were considered semitransparent because a part of the incident radiation reflects and part of it transmits through the walls. Lasers in general emit beams that are approximated by a Gaussian profile, but in the model, a circular beam of uniform intensity profile is considered. The value of irradiation due to the laser beam was calculated by dividing the power of the laser beam with the cross-section of the beam (or the area of the Wall 1) and applied as direct irradiation on Wall 1. Using the values of $\theta = 1x10^{-6}$ and $\phi = 1x10^{-6}$ in the beam width option, the beam was described as a collimated radiation. The direction of the beam was given using direction vectors (x,y,z) of the centroid of the solid angle. The diffuse fraction determines the dispersion of the reflected and refracted parts of the radiation and ranges from 0 (complete specular) to 1 (complete diffuse). Passing a laser light through a test tube with water revealed that most of the light was concentrated at the center, so a diffuse fraction value of 0.1 was applied for the exterior and interior walls to minimize the dispersion of transmitted radiation.

All the walls were given zero wall thickness as the tube wall thickness itself was modeled as a solid zone participating in radiation. The exterior walls were subjected to a convective boundary condition in which the free stream temperature (room temperature = 25^0 C) and the heat transfer coefficient (15 W/m^2K) were given [27]. The two-sided interior walls were coupled so that the solver calculates the heat transfer directly from the solution in the adjacent cells.

4.3.5 Solution Strategies and Solver Specifications

Solution strategies and solver specifications are used to control the convergence and accuracy of solution. For the current model and simulation which does not involve any fluid flow, most of the solution strategies and solver specifications were set to their default values in FLUENT. When the DO model is active, FLUENT updates the radiation field during calculation and computes resulting energy sources and heat fluxes. The flow iterations per radiation iteration are used to control the frequency with which the radiation field is updated as continuous phase solution proceeds. Since radiative transfer is the dominant mode of heat transfer in the current model, the flow iterations per radiation iteration were set to 1. Then, the solution was initialized at room temperature. With these settings, the solution was iterated until it meets the default convergence criterion for both DO and energy equations.

4.4 Results and Discussion

There are numerous postprocessing options in FLUENT. The important ones that are made use of in analyzing the current problem are:

a. Contours of static temperature that show the 3D profiles of temperature distribution along with the minimum and maximum values of the variable

b. XY plots that yield the temperature distribution or radiant intensity along a specified direction

c. Flux reports that yield the radiative heat transfer rates.

A number of simulations were run for different geometries considering only the fluid zone, both solid and fluid zones, for different wavelengths, by varying the incident irradiation flux (input power), and by varying the time of irradiation. To explain the basic results, an example of the generic model containing both solid and fluid zones is considered. For the generic model, the domain is irradiated normal to the surface, in X direction, with a 980 nm laser beam of power 500 mW and with a beam diameter of 2 mm for 5 seconds. Temperature distribution and transmitted radiation intensities are explained for this generic model.

4.4.1 Temperature Distribution

Figure 4.5 shows the temperature distribution profiles superimposed on the physical domain of the model. It shows that the maximum temperature is 304 K which is at the boundary where the irradiation occurs and decreases as we move away from the point of incidence.

Since the domain is a cylindrical 3D element, XY plots are used to better understand the temperature distribution. Figure 4.6 shows the variation of temperature against the position in X direction. It shows that maximum temperature is at the point of incidence and decreases along the path of light. Moving away from the beam of light in Y or Z directions results in lower temperature profiles. From these plots, temperature at any point in the domain can be determined. The domain extends from -0.0076 m to 0.0076 m with the fluid zone in the range -0.006 m to 0.006 m and the remaining solid zone.

4.4.2 Transmitted Radiation

Using the XY plots, the incident radiation is plotted against dimensions of the domain in X, Y, and Z directions to understand the variation of incident radiation in the desired direction. Figure 4.7 shows the decay in intensity of incident radiation along the path of light in X direction. For the fluid zone which extends from -0.0065 m to 0.0065 m, the exponential decay of incident radiation is observed.

The radiation heat transfer rates through various boundaries are reported using the flux reports in FLUENT. The positive sign in the flux reports denotes flux entering and the negative sign indicates flux leaving the boundaries. From Table 4.2, radiation heat transfer rates imply that through Wall 1 (wall of incidence), 461.53 mW power of incident radiation enters, 171.68 mW is transmitted through Wall 2, and the net value represents that 244.28 mW of power is absorbed by the semitransparent media water and polypropylene. It also shows that radiative transfer on remaining walls is negligible.

4.4.3 Comparison of FLUENT Model with Beer-Lambert Law

To verify the correctness of the model, a simple rectangular geometry shown in Figure 4.8 was modeled with only fluid zone as water. The homogeneous medium is irradiated with a collimated monochromatic radiation of narrow beam. Scattering was assumed negligible and with the non-gray implementation, even the emission was neglected. Beer-Lambert's law of absorption is written as

$$\frac{I}{I_0} = e^{(-aL)}$$

where I and I_0 are the intensities of incident and transmitted light, a is the absorption coefficient, and L is the distance through which light moves through the medium.

In Figure 4.9, the decrease in intensity of incident radiation according to the FLUENT simulation is compared with the Beer-Lambert's exponential decay of incident radiation along the path length, which shows the consistency of the model.

4.4.4 Experimental Validation of Transmitted Radiation

The radiant power of transmitted radiation obtained from the simulation is validated using the available experimental equipment. The experimental set-up and conditions were similar to the ones that were used for detection of interferences using LDs. The detector PDA36A was replaced with a photo-diode sensor PD300-1W in conjunction with an OPHIR NOVA 11 power meter, as shown in Figure 4.10. PD300-1W is a photodiode power sensor with automatic background subtraction. The detector has a 10x10 mm aperture and detects light in the spectral range of 410 nm - 1100 nm and a power range of 200 µW to 1 W. A polypropylene tube with de-ionized water was used and the experiment was conducted with the available 3 LDs of wavelengths 532 nm, 690 nm, and 980 nm.

Several uncertainties are possible in the experiments, so to compare the results from experiments and simulations, an uncertainty analysis was conducted.

The power output of the LDs is monitored by the photodiode current. The diameter of the laser beam differs with different LDs used. The divergence of the beam is minimized by allowing minimum separating distance between the light source, tube, and the detector. The laser beam has a Gaussian profile but is approximated as a circular beam of uniform intensity in the simulation. The tube diameter and wall thickness vary at micron level. There may be uncertainty in the absorption coefficients of water used in the simulation. The aperture of the photodiode sensor is approximated as a face on the

cylindrical geometry. Calibration of the detector must account for the spectral sensitivity and linearity of detectors. Uncertainties that cause significant differences between experiments and simulations are quantified as follows.

The photodetector used is linear but has large variation in sensitivity with wavelength. The maximum error in the measurement including the calibration accuracy, linearity of detectors, variations in sensitivity with wavelength, and variations in gain with temperature is +/-5% in the wavelength range 430 nm – 950 nm and +/-7% in 950 nm – 1100 nm range. Using these percentage error values, the lower and upper bound values were determined for the incident power measured in experiment.

The diameter of the laser beam ranges from 1 mm to 3 mm for the LDs used. From the FLUENT simulation, it was observed with an increase in diameter of beam or wall, the radiant power of transmitted radiation increases. So the lower and upper bound values of beam diameter considered were 1 mm and 3 mm.

The light transmitted through the tube with water is detected by a photodiode power sensor that is aligned as close as possible to the test tube. From the FLUENT simulations, it was found that the radiant power of transmitted radiation increases with the diameter of the wall. The photodiode has an aperture of 10x10 mm so the maximum and minimum diameters of the wall through which transmitted radiant power is measured were considered as 10 mm and 8 mm, respectively.

To compare the results from experiments and simulations, the model was simulated for the combination of these lower and upper boundary levels for each of the experiments conducted. The lower boundary values (LBV) are -5% or -7% (based on wavelength of LD) of the incident power, 1 mm for Wall 1 diameter, 8 mm for Wall 2 diameter, and the

upper boundary value (UBV) is +5% or +7% of the incident power, 3 mm for Wall 1 diameter, and 10 mm for Wall 2 diameter. The geometry was changed according to the required wall diameters.

The same model settings were used for these simulations except for the convergence criterion, which was increased from 10^{-6} to 10^{-8} for better accuracy. The comparison of experimental results against simulation results, including the uncertainties, is presented in Table 4.3. The table shows that the radiant power of transmitted light measured in experiment falls in the range of power values determined from the simulations for LBV and UBV. So the experimental and simulation results are in good agreement.

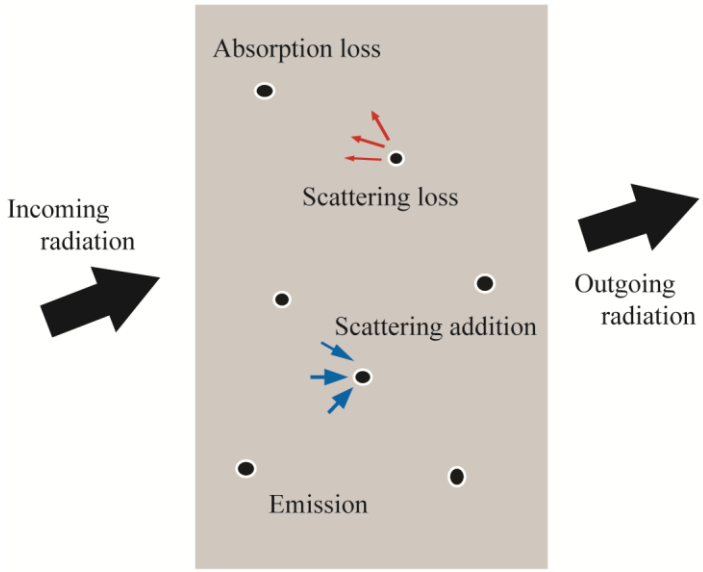

Figure 4.1 Radiative transfer through participating medium involves absorption, in-scattering, out scattering, and emission.

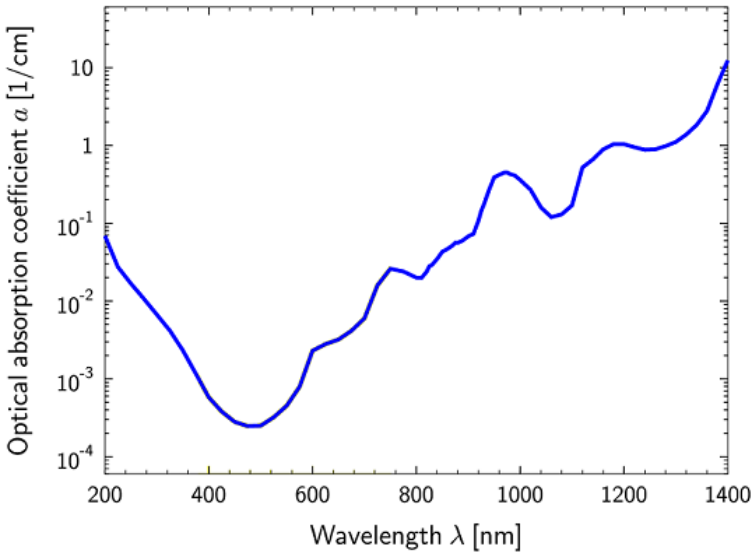

Figure 4.2 Optical absorption coefficient of water [24]

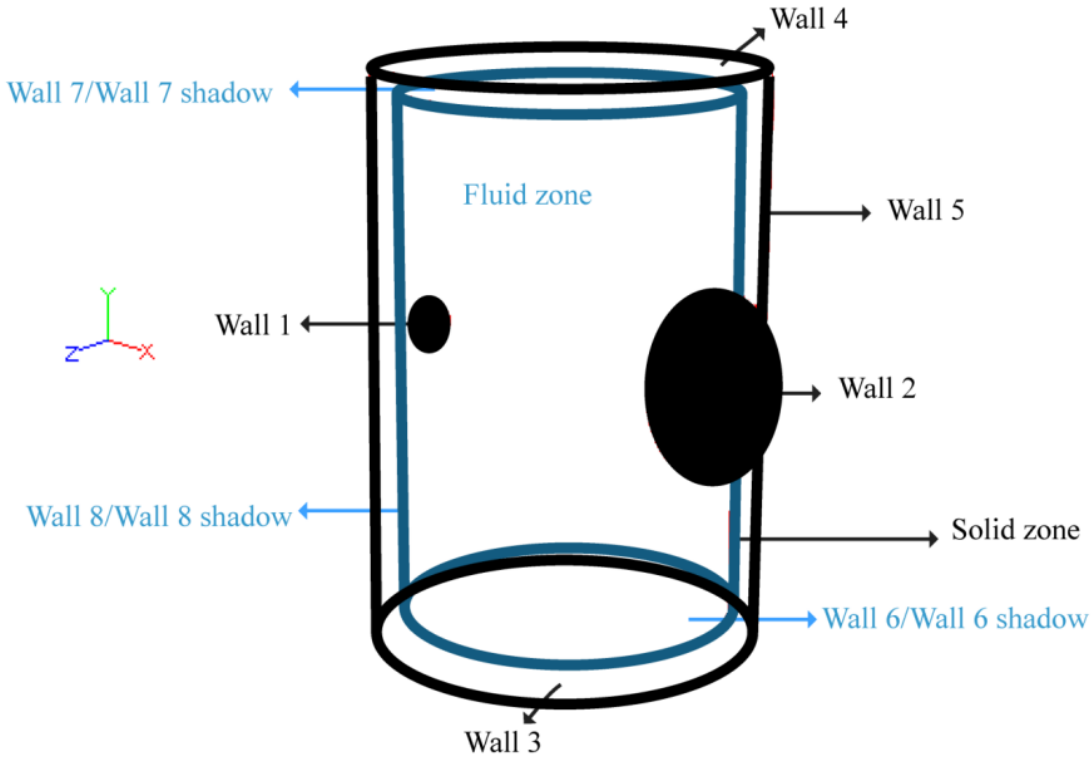

Figure 4.3 Model geometry showing the interior and exterior walls and fluid and solid zones.

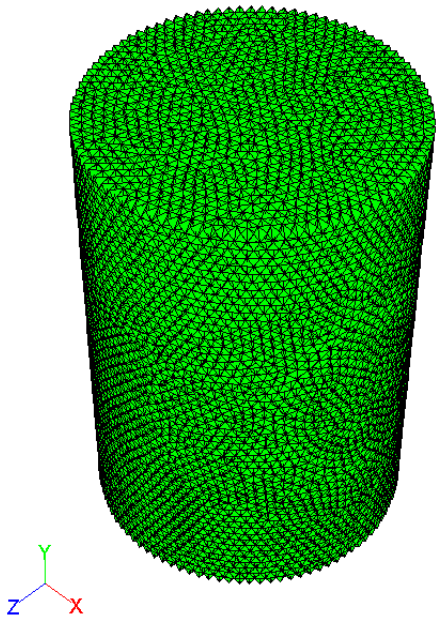

Figure 4.4 Meshed geometry

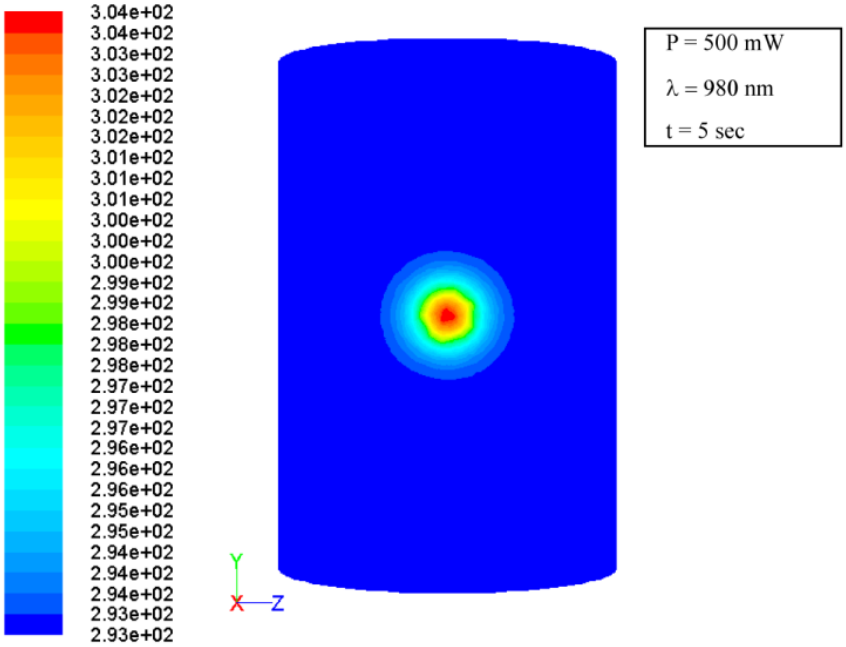

Figure 4.5 Contours of static temperature

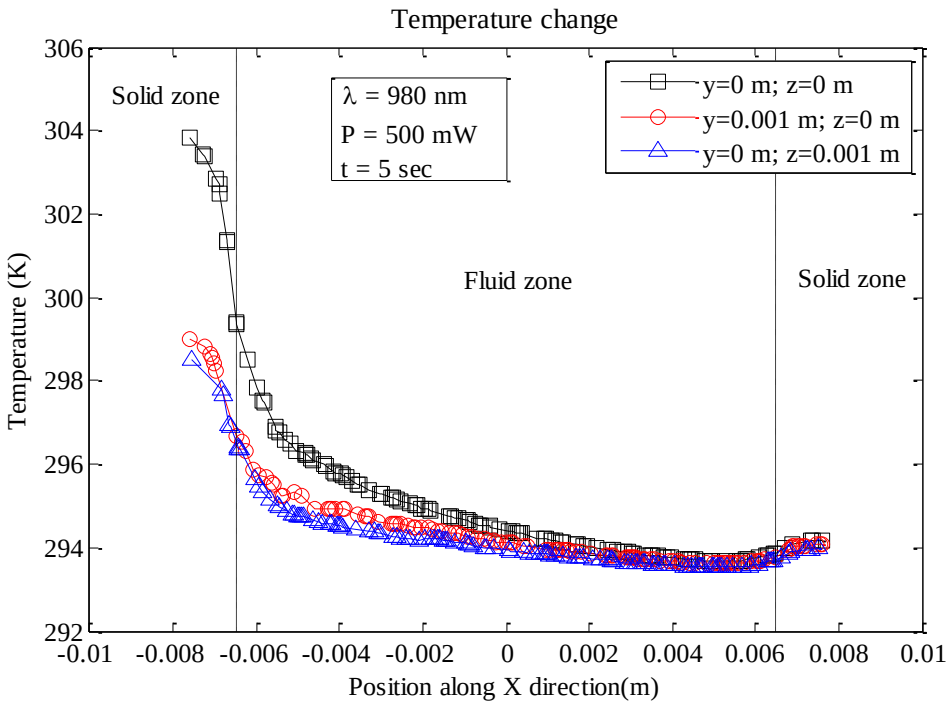

Figure 4.6 Decrease of temperature in the X direction

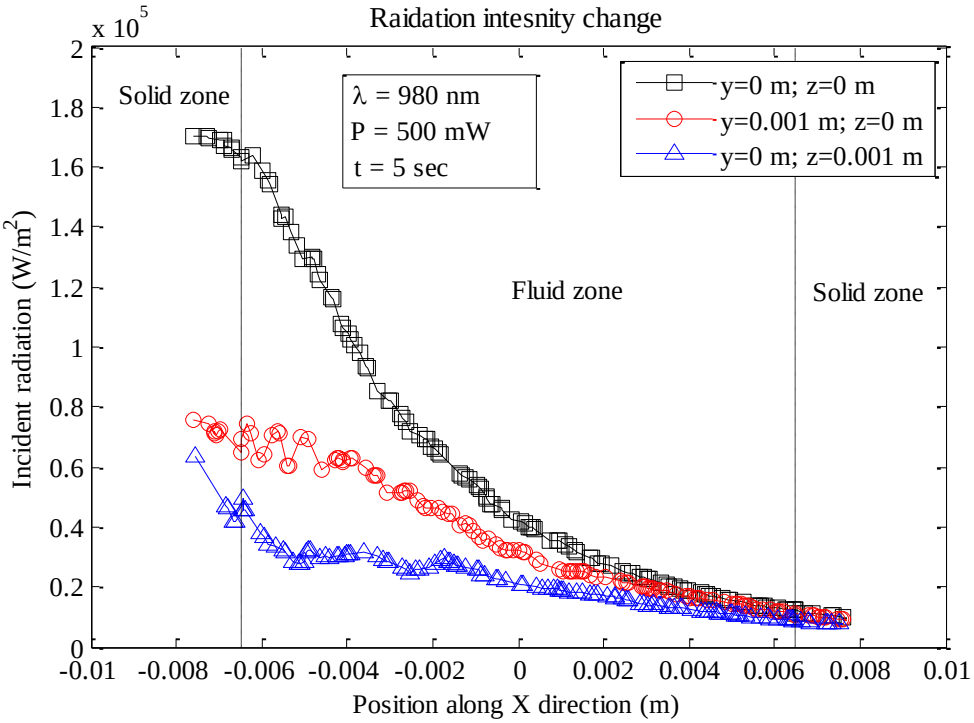

Figure 4.7 Transmitted radiation along the X direction

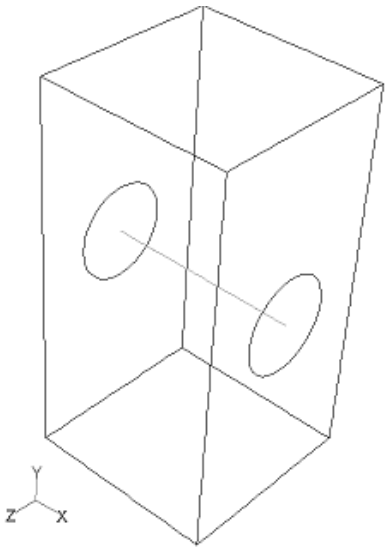

Figure 4.8 Geometry used in FLUENT simulation to compare with Lambert's law

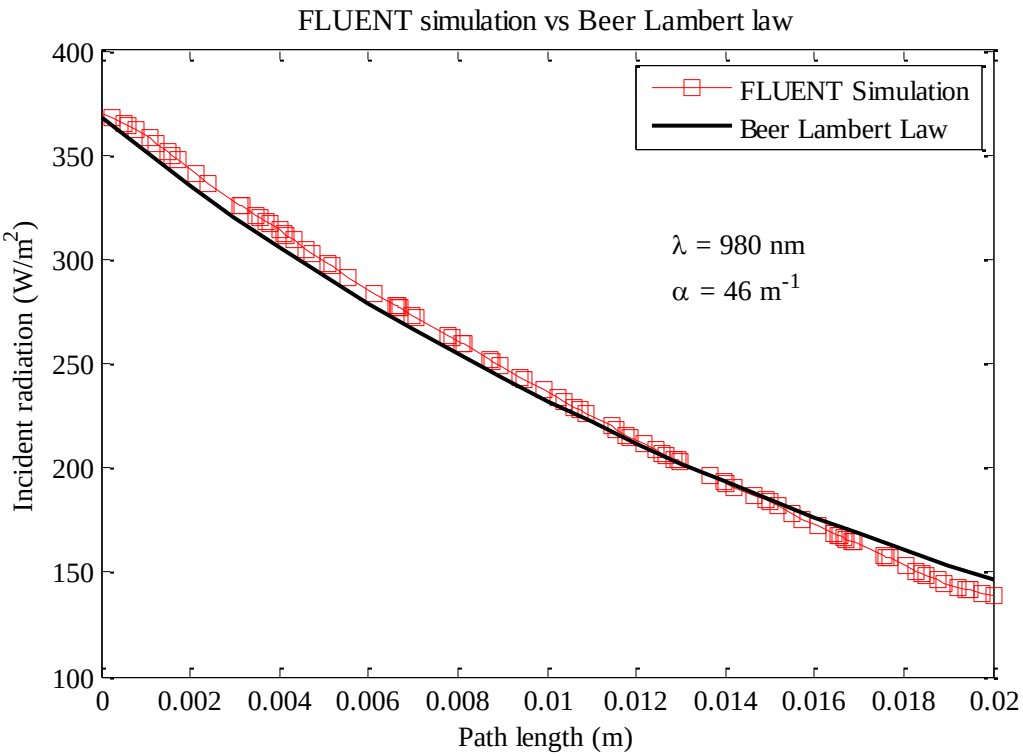

Figure 4.9 Comparison of FLUENT model with Lambert's law

Figure 4.10 Power meter and photodiode used in the experimental validation [28]

Table 4.1 Optical thicknesses of water and polypropylene tube [5], [25], [26]

Wavelength (nm)	Absorption coefficient of water (m^{-1})	Optical thickness of water	Absorption coefficient of tube (m^{-1})	Optical thickness of tube
980	46	0.598	60	0.06
690	0.5278	6.8×10^{-3}	145.3	0.1453
532	0.0028	3.64×10^{-5}	251.4	0.2514

Table 4.2 Radiation heat transfer rate from flux reports

Boundary Id	Radiation Heat Transfer Rate (Watts)
Wall 1	0.46153018
Wall 2	-0.17168081
Wall 3	-5.575634e-07
Wall 4	-5.4908782e-07
Wall 5	-0.045562129
Wall 6	2.1306148e-05
Wall 6 shadow	-2.1306148e-05
Wall 7	2.1147933e-05
Wall 7 shadow	-2.1147933e-05
Wall 8	-0.19795376
Wall 8 shadow	0.19795376
Net	0.24428613

Table 4.3 Comparison between experimental and simulation results

Wavelength of LD used (nm)	Incident power measured in power meter (mW) (LBV,UBV)	Transmitted power measured in power meter (mW)	Radiant power of transmitted light from simulation for LBV (mW)	Radiant power of transmitted light from simulation for UBV (mW)
980	4.12 (3.8316,4.4084)	1.65	1.307	1.84
690	14.05 (13.3475,14.7525)	7.05	6.98	9.44
532	39.96 (37.962,41.958)	20.23	16.02	21.62

CHAPTER 5

CONCLUSIONS AND FUTURE SCOPE

5.1 Conclusions

The optical signatures for Hemolysis, Icterus, and Lipemia were obtained. The absorption spectra are analyzed and optimal pairs of absorption and reference wavelengths are identified in Table 5.1.

A novel optical measurement system was developed to measure concentrations of interferences in serum samples by computing the power ratios of transmitted light for absorption and reference wavelengths. The system is capable of measuring concentrations of Hemolysis, Icterus, and Lipemia up to 1250 mg/dL, 60 mg/dL, and 707 mg/dL, respectively, for test tubes without labels.

To model the temperature distribution and to determine the power of transmitted radiation through a liquid sample irradiated by a laser beam, a radiative heat transfer model is formulated. The transmitted radiation results are experimentally validated for water in a test tube using the available laser light sources.

5.2 Future Scope

The next phase of research would be to improve the measurement system for higher concentrations. This requires scattering corrections to be included in the study of transmission or attenuation of light. The current research is limited to test tubes without

labels; similar experiments have to be conducted for different label combinations attached on the outside of the tube. Finally, a proto-type has to be designed and developed that could be used in ARUP Labs to automatically measure concentrations of interferences in serum samples.

The radiative heat transfer model formulated in Chapter 4 is applied for water in a test tube, while the biological samples contain blood plasma or serum. Pure water is considered to be particle free, but the biological samples contain particles and so scattering must be considered for accurate results. Blood plasma mainly contains water (93% by volume) and contains dissolved proteins, glucose, mineral ions, hormones, carbon dioxide, and clotting factors. Blood serum is blood plasma without fibrinogens (cells) and clotting factors [29]. The properties (physical, thermal, optical, and radiative) of serum have to be studied and included in the model to understand the effects of absorption and scattering and to determine the temperature distribution and transmitted power of radiation. Also, the labels that reflect and absorb a large amount of light must be modeled as a layer on the tube. The results can be used to determine the required power of light sources to be used in the measurement system.

Table 5.1 Optimal pairs of absorption and reference wavelengths

Interference	**Absorption wavelength, $\lambda_{a\,(nm)}$**	**Reference wavelength, $\lambda_{r\,(nm)}$**
Hemolysis	532	690
Icterus	525	570
Lipemia	690	980

REFERENCES

[1] Charles W Hawker, "Private communication," 2012.

[2] "ARUP Laboratories - Automation Initiative." [Online]. Available: http://www.aruplab.com/LaboratoryExpertise/AutomationInitiative/index.jsp. [Accessed: 10-Jan-2012].

[3] X. Liu, "Optical System to Evaluate Volume of Medical Samples," University of Utah, 2011.

[4] X. Liu, B. J. Corbin, S. J. Morris Bamberg, W. R. Provancher, and E. Bamberg, "Optical system to detect volume of medical samples in labeled test tubes," *Optical Engineering*, vol. 47, no. 9, p. 094402, 2008.

[5] X. Liu, S. J. M. Bamberg, and E. Bamberg, "Increasing the accuracy of level-based volume detection of medical liquids in test tubes by including the optical effect of the meniscus," *Measurement*, vol. 44, no. 4, pp. 750-761, May 2011.

[6] Linda D. Lemery, "Oh, No! It's Hemolyzed!," 1988.

[7] "Jaundice." [Online]. Available: http://www.ncbi.nlm.nih.gov/pubmedhealth/PMH0001259/. [Accessed: 2012].

[8] A. Gotto, *The Cornell Illustrated Encyclopedia of Health*. Washington DC: Lifeline Press, 2002.

[9] L. Rovati and F. Docchio, "Determination of the concentrations of interferents in blood serum by use of a novel solid-state colorimeter," *Measurement Science and Technology*, vol. 11, p. 185, 2000.

[10] M. R. Glick, K. W. Ryder, S. J. Glick, and J. R. Woods, "Unreliable visual estimation of the incidence and amount of turbidity, hemolysis, and icterus in serum from hospitalized patients.," *Clinical Chemistry*, vol. 35, no. 5, pp. 837-839, 1989.

[11] S. Gunasekaran and D. Uthra, "FTIR and UV-Visible Spectral Study on Normal and Jaundice Blood Samples," *Asian Journal of Chemistry*, vol. 20, no. 7, pp. 5695–5703, 2008.

[12] M. Thirunavukkarasu, “FTIR and UV-visible spectral study on normal blood samples,” *International Journal of Pharmaceutics*, vol. 1, no. 2, 2011.

[13] H. Ranganathan and N. Gunasekaran, “Simple method for estimation of hemoglobin in human blood using color analysis.,” *IEEE transactions on information technology in biomedicine : a publication of the IEEE Engineering in Medicine and Biology Society*, vol. 10, no. 4, pp. 657-62, Oct. 2006.

[14] T. B. D. Campbell, J. Luoma, J. Seago, “Reduced Turnaround Time for Hemolysis/Icterus/Lipemia (HIL) Interferent Indices on ARCHITECT Chemistry Analyzers,” in *American Association for Clinical Chemistry Annual Meeting*, 2007.

[15] F. Neudel, S. Takatani, H. Reul, and G. Rau, “Effect of hemolysis on oxygen and hematocrit measurements by near infrared reflectance spectroscopy.,” *Medical Engineering & Physics*, vol. 24, no. 4, pp. 301-307, 2002.

[16] Y. Sankai, T. Tsutsui, T. Jikuya, O. Shigeta, M. Ohta, and T. Mitsui, “Method of noninvasive and continuous hemolysis/thrombogenesis measurement by laser photometry during artificial heart development.,” *ASAIO journal American Society for Artificial Internal Organs 1992*, vol. 43, no. 5, p. M682-M686, 1997.

[17] R. (IL) Ilya Fine and J. (IL) Leonid Shvartsman, “Method of optical measurement for determing various parameters of the patient’s blood,” 23-Mar-2004.

[18] D. Swinehart, “The beer-lambert law,” *Journal of Chemical Education*, vol. 39, no. 7, pp. 333-335, 1962.

[19] “Beer-Lambert Law.” [Online]. Available: http://en.wikipedia.org/wiki/Beer%E2%80%93Lambert_law. [Accessed: 11-Mar-2012].

[20] J. Qin and R. Lu, “Measurement of the absorption and scattering properties of turbid liquid foods using hyperspectral imaging,” *Applied spectroscopy*, vol. 61, no. 4, pp. 388–396, Apr. 2007.

[21] C. F. Bohren and D. R. Huffman, *Absorption and scattering of light by small particles*, vol. 1, no. 1. Wiley, 1983, p. xiv, 530 p.

[22] M. F. Modest, *Radiative Heat Transfer*, vol. 18, no. 3. Academic Press, 2003, p. 822.

[23] “Ansys fluent 12.0 Documentation,” no. April. 2009.

[24] “Absorption_purewater.” [Online]. Available: http://hossenfelder.tigblog.org/post/580209. [Accessed: 03-Oct-2011].

[25] G. M. Hale and M. R. Querry, “Optical Constants of Water in the 200-nm to 200-microm Wavelength Region.,” *Applied optics*, vol. 12, no. 3, pp. 555-63, Mar. 1973.

[26] C. W. Robertson and D. Williams, “Lambert Absorption Coefficients of Water in the Infrared,” *Journal of the Optical Society of America*, vol. 61, no. 10, p. 1316, Oct. 1971.

[27] A. S. L. Frank P. Incropera, David P. DeWitt, Theodore L. Bergman, *Fundamentals of Heat and Mass Transfer*, Sixth. Wiley, 2006.

[28] L. Power and E. Meter, “NOVA || USER MANUAL.”

[29] “Blood Plasma.” [Online]. Available: http://en.wikipedia.org/wiki/Blood_plasma. [Accessed: 02-Oct-2012].